ACADEMIC PRESS

Available online at www.sciencedirect.com

SCIENCE DIRECT®

Icarus 162 (2003) 74–93

ICARUS

www.elsevier.com/locate/icarus

The dynamics of jovian white ovals from formation to merger

Ashraf Youssef and Philip S. Marcus*

Department of Mechanical Engineering, University of California—Berkeley, Berkeley, CA 94720, USA

Received 1 November 2000; revised 6 August 2002

Abstract

In early 1998 two of the three, long-lived anticyclonic, jovian white ovals merged. In 2000 the two remaining white ovals merged into one. Here we examine that behavior, as well as the dynamics of three earlier epochs: the Formation Epoch (1939–1941), during which a nearly axisymmetric band broke apart to form the vortices; the Kármán Vortex Street Epoch (1941–1994), during which the white ovals made up the southern half of two rows of vortices, and their locations oscillated in longitude such that the white ovals often closely approached each other but did not merge; and the Pre-merger Epoch (1994–1997), during which the three white ovals traveled together with intervening cyclones from the northern row of the Kármán vortex street in a closely spaced group with little longitudinal oscillation. We use a quasi-geostrophic model and large-scale numerical simulation to explain the dynamics. Our models and simulations are consistent with the observations, but none of the observed behavior is even qualitatively possible without assuming that there are long-lived, coherent cyclones longitudinally interspersed with the white ovals. Without them, the white ovals approach each other and merge on a fast, advective timescale (4 months). A necessary ingredient that allows the vortices to travel together in a small packet without spreading apart is that the strong, eastward-flowing jetstream south of the white ovals is coincident with a sharp gradient in background potential vorticity. The jet forms a Rossby wave and a trough of the wave traps the white ovals. In our simulations, the three white ovals were trapped before they merged. Without being trapped, the amount of energy needed to perturb two white ovals so that they merge exceeds the atmosphere's turbulent energy (which corresponds to velocities of $\sim$1 m s^{-1}) by a factor of $\sim$100. The mergers of the white ovals BC and DE were not observed directly, so there is ambiguity in labeling the surviving vortices and identifying which vortices might have exchanged locations. The simulation and modeling make the identifications clear. They also predict the fate of the surviving white oval and of the other prominent jovian vortex chains.

Keywords: Jupiter; Atmosphere; Dynamics; White oval spots

1. Introduction

Prior to 1998 the three white ovals BC, DE, and FA, shown in Fig. 1, were part of a chain of jovian anticyclones located at approximately 33°S[1] latitude and were the most obvious features on the planet after the Great Red Spot (GRS). The three white ovals formed in the late 1930s. They are bright and compact, and like the GRS, they are embedded in an anticyclonic, shearing east–west wind. Due to the similarities in appearance and behavior, they were treated as "mini Red Spots" and were therefore believed to be long-lived and perhaps permanent. To the surprise of many, the two white ovals BC and DE merged into a single anticyclone some time between November 1997 and March 1998, and the combined vortex BC + DE merged with FA in 2000. In this paper numerical simulations and theoretical analyses are used to explain the merger and the events that led to it, as well as implications for the fate of the surviving vortex. We believe that our study coupled with the new observations will lead to a deeper understanding of the jovian atmosphere, which has many rows of anticyclones.

The white ovals have exhibited four distinct types of behavior over time, and the names that we use to describe them are of our own coinage. The first is the Formation

* Corresponding author. Department of Mechanical Engineering, University of California—Berkeley, Berkeley, California 94720.

E-mail address: pmarcus@newton.berkeley.edu (P.S. Marcus).

[1] Throughout this article latitudes are planetographic.

0019-1035/03/$ – see front matter
doi:10.1016/S0019-1035(02)00060-X

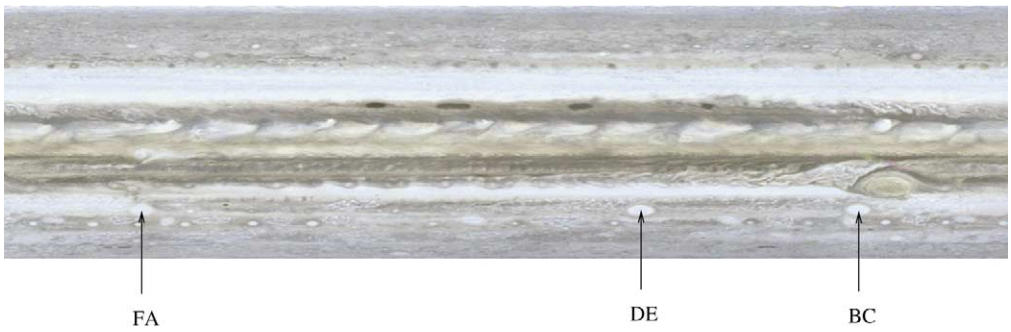

Fig. 1. A cylindrical projection (Smith et al., 1979) of Jupiter extending around the entire planet taken by *Voyager 1* on 1 February 1979. The image extends from 60°S to 60°N in latitude.

Epoch (1939–1941), during which a band of clouds in the South Tropical Zone (STZ) broke apart to form three elongated vortices. In the Kármán Vortex Street Epoch (1941–1994), the locations of the white ovals had large east–west oscillations during which there were nearly a dozen close approaches between pairs of white ovals interspersed with periods of large separations. During the Pre-merger Epoch (1994–1997), the white ovals drifted toward each other and traveled eastward together along with other vortices as a tightly spaced packet without oscillations. The Merger Epoch (1997–2000) is characterized by the merger of white ovals BC and DE and then BC + DE with FA.

Our paper is organized as follows. Section 2 contains a summary of the observations that we believe are relevant to the dynamics of the vortices such as drift speeds and wind velocities. We do not discuss such things as color, composition, temperature, or albedo, which we do not believe play causal roles in the dynamics. In Section 3 we review the properties of planetary vortex dynamics that we believe are fundamental in interpreting the white ovals, and in Section 4 we provide numerical illustrations of those dynamics. In Section 5 we apply these to the white ovals. Our discussion, predictions of future behavior, and suggestions for observations are in Section 6.

2. Observations

2.1. Formation epoch (1939–1941)

As summarized by Rogers (1995), before 1939 there was an axisymmetric band of clouds that circled Jupiter near 34°S latitude. During 1939, this band broke into three approximately equal sections to form BC, DE, and FA. These "proto-ovals" initially contracted rapidly in longitude, and by late 1940 the average longitudinal lengths of BC and DE were approximately 90° while that of FA was approximately 75°. Since their creation in 1939, the white ovals have drifted eastward around the planet at progressively slower speeds. In the early 1940s, their speeds[2] were ~ 7 m s^{-1}.

2.2. Kármán Vortex Street Epoch (1941–1994)

In this epoch, the anticyclones were arranged in a row at the same latitude with intervening, cyclonic filamentary regions (vortices) slightly to their north. A flow such as this, where there are two parallel, staggered rows of vortices with opposite senses of rotation, is known as a Kármán vortex street. The cyclonic regions and white ovals were embedded in a global east–west flow with strong shear such that the clouds associated with the cyclonic regions were embedded in a cyclonic belt while the anticyclonic white ovals were embedded in an anticyclonic zone. This epoch was characterized by large-amplitude oscillations of the longitudinal positions of the white ovals.

After 1940, the white ovals continued to contract in longitude, and by 1960, all three had east–west lengths of $\sim 20°$ (Rogers, 1995). In 1979 the white oval BC, which had generally been the largest of the three, had an east–west diameter of 10° to 11.4° (12,000 to 14,000 km) and a north–south diameter of 5° (6,200 km), giving it an aspect ratio of about 2:1. Ovals BC and DE remained $\sim 8°$ long throughout the 1980s, while FA shrank to $\sim 5°$ by 1988 (Rogers and Herbert, 1991). In contrast, throughout all epochs, the latitudinal extent of each of the white ovals has been constant, between 5° and 7° (Rogers, 1995).

The average eastward drift rate of the white ovals decreased steadily from ~ 7 m s^{-1} in 1940 to ~ 3 m s^{-1} in 1992. During that same time the white ovals moved northward $\sim 2°$ and became rounder. The maximum rotational velocity within BC during the 1979 *Voyager* encounters was 120 ± 5 m s^{-1} (Mitchell et al., 1981). From a dynamical point of view, the most striking aspect of the Kármán Vortex Street Epoch was the large, but irregular oscillations

[2] With respect to System III, a coordinate system rotating with the interior of the planet, which has a period of 9h 55m 29.7s as determined from radio observations.

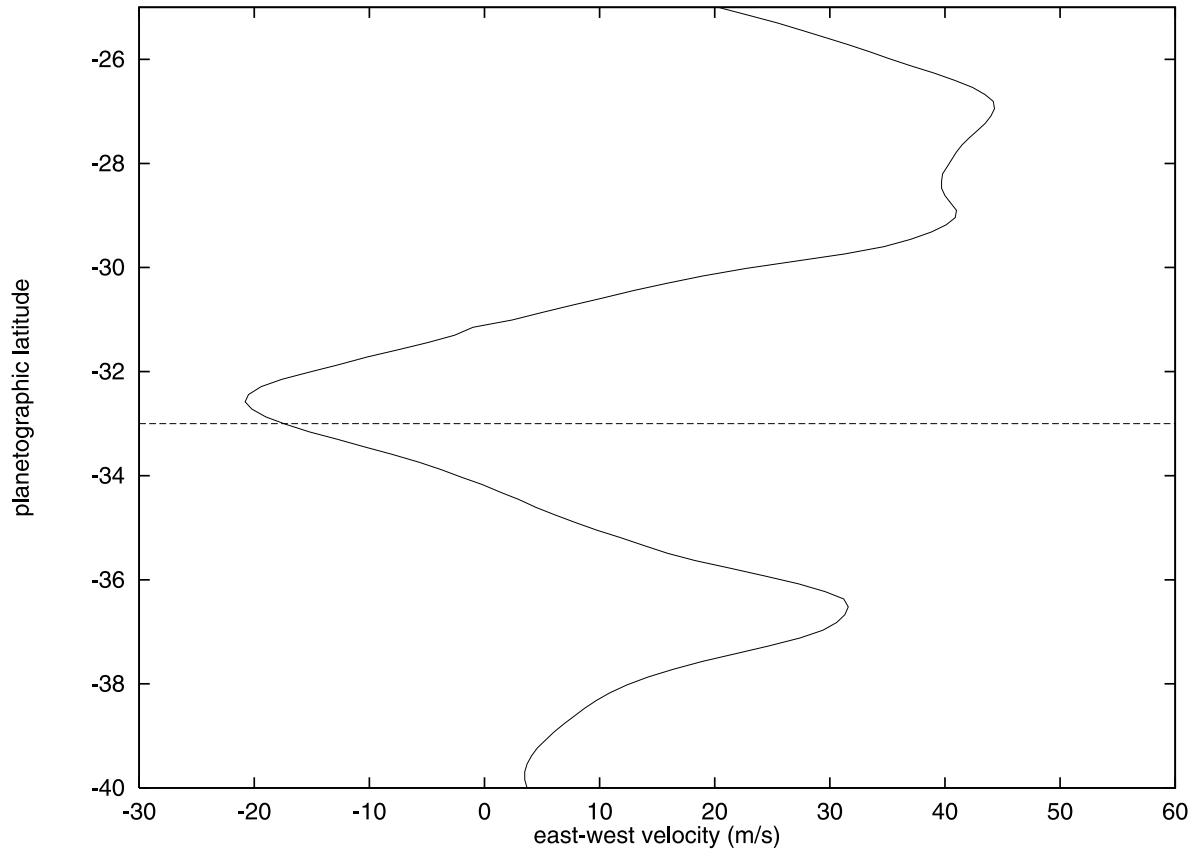

Fig. 2. The solid curve is the average jovian east–west velocity $u(y)$ during the *Voyager* encounters as a function of latitude y (Limaye, 1986). The average latitude of the three white ovals during this same time is shown with the dashed line.

in the longitudinal locations of the white ovals. Several times, two white ovals were separated by only a few of their diameters; other times, they were nearly equally spaced around the planet. For example, during the *Voyager* missions in 1979 the separations were large; FA was 55° to the east of BC. By 1987, FA was 160° east of BC and DE was 60° west of BC (Beebe et al., 1989). Later the longitudinal separations decreased. In 1988 the separation between the centers of BC and DE shrank to ∼17° (Kuehn and Beebe, 1989), and that between BC and DE was 22° in 1988–1989 and 18° in 1990–1992.

During this epoch, each time two white ovals approached each other they always appeared to "repel" when their separations became sufficiently close (although the times at which a pair began to repel did not always correspond to a small separation). Sato fitted the longitudinal separation S of a pair of white ovals and their accelerations to Hooke's law superposed on a uniform repulsion: $d^2S/dt^2 = -3.8\,10^{-10}\,S + 4.6 \times 10^{-8}$, using MKS units (Sato, 1974). Sato's data were mostly for instances of widely separated vortices, and his data had a great deal of scatter. Moreover, no theoretical argument was postulated for choosing Hooke's law (see Section 3.5). The vortex oscillations raise an interesting question: why did the white ovals repel each other (and not merge until 1998), since simulation and theory of the quasi-geostrophic (QG) equations show that two like-signed vortices that are either in close proximity to each other or embedded in the same east–west shear flow tend to attract each other and merge (Ingersoll and Cuong, 1981; Marcus, 1993)? The fact that vortices at the same latitude computed with the QG equations tend to all merge with each other leaving only a single large vortex (cf. the Red Spot) was cited as an advantage of the QG theory over other GRS models in which the vortices did not merge, such as solitary wave models (Ingersoll and Cuong, 1981). However, in modeling the jovian vortex streets with the QG equations, the apparent inability to prevent the vortices from merging is a problem.

Theory and simulation show that vortices are influenced by the winds in which they are embedded. The ambient east–west wind velocity $u(y)$ near the white ovals has a shear $\sigma(y) \equiv -du/dy$ that changes with latitude y. Fig. 2 shows that the centers of the white ovals are located near, but just south of, the peak of a westward jet at 32.6°S with velocity 21 m s^{-1} and well north of an eastward jet at 36.5°S with velocity of 32 m s^{-1}. The cyclones that make up the northern part of the Kármán vortex street are north of the westward jet at 32.6°S and south of an eastward jet at 28.9°S (Limaye, 1986). Although $\sigma(y)$ changes sign at the latitude of the westward jet, it is surprisingly uniform over

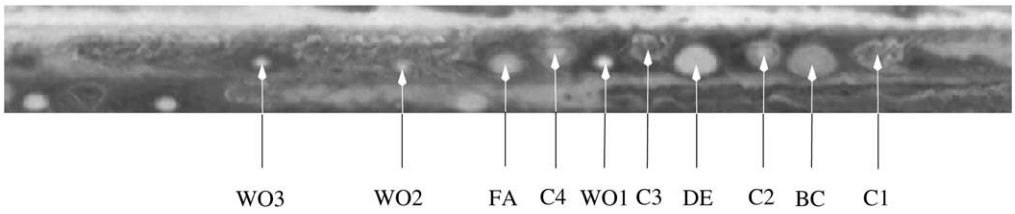

Fig. 3. A mosaic (Simon et al., 1998) centered at 33°S latitude taken by the Hubble Space Telescope (HST) on 21 October 1996 showing the anticyclonic white ovals (BC, DE, and FA), smaller anticyclones (WO1, WO2, and WO3), and the cyclonic regions between them (C1, C2, C3, and C4). The mosaic spans ±10° in latitude and 180° in longitude.

most latitudes spanned by the white ovals, with $\sigma(y) = 1.1 \times 10^{-5}$ s^{-1}. Over the latitudes spanned by the cyclones, $\sigma(y) = -1.6 \times 10^{-5}$ s^{-1}.

Although there have been many observations of cyclonic regions between and north of the white ovals, their interpretation is controversial. The cyclones' large east–west extent, filamentary clouds, and rapid morphological changes have cast doubts as to whether the regions are either long-lived or even associated with coherent vortices. The general consensus is that they are neither. Despite repeated observations of "cyclonic filamentary regions" in the *Voyager* images, MacLow and Ingersoll (1986) concluded that "90% of the stable long-lived spots [Jovian vortices] are anticyclonic," and this statement is consistently cited in the literature, cf. Nezlin (1994), Sutyrin (1994), and Ingersoll (1996). We challenged this interpretation earlier (Marcus, 1993) and shall rechallenge it again in Section 5 where we argue that the white ovals would have quickly (within a year) merged into one large vortex unless the three intervening cyclonic regions were stable and long-lived (of order the 60 years that the vortex street containing the white ovals existed).

2.3. Pre-merger epoch (1994–1997)

During the years 1994–1997, the white ovals along with other vortices at 33°S moved within a few diameters of each other and maintained nearly constant spacing, traveling eastward as a tight packet. This is the epoch-defining characteristic. Fig. 3, taken on 21 October 1996, shows three smaller anticyclones, labeled as WO1, WO2, and WO3, at the same latitude as white ovals BC, DE, and FA. Also shown are the intervening cyclonic regions labeled C1, C2, C3, and C4 (our nomenclature), which exhibit the signature filamentary structure of most other jovian cyclones.

In 1997, white oval BC was 8° (9800 km) in longitude by 6° (7400 km) in latitude (Simon et al., 1998). The *Galileo* data showed that the maximum rotational velocities of BC and C2, the cyclonic system between BC and DE, were 120 ± 20 m s^{-1}. The turnaround time for BC was approximately 3 days. (In comparison, the GRS is 24,000 × 14,500 km^2 with a turnaround time of 6–8 days and a maximum rotational velocity of 110 ± 12 m s^{-1} (Mitchell et al., 1981).) By 1997 the eastward drift velocity of all three white ovals slowed to 1.6 ms^{-1} (Simon et al., 1998).

When the spacing between white ovals BC and DE shrank to 18° in 1990–1992, they began traveling east as a group with the cyclonic region C2 between them (Rogers, 1995). The small anticyclone WO1 also traveled with them, and in late 1995 FA joined them. The remarkable dynamical feature of this epoch is that the Kármán vortex street traveled as a closely spaced unit for nearly four years without spreading apart. The spacing between the centers of the anticyclones was approximately 19,000 km (which is ~10 Rossby deformation radii at this latitude).

The tight confinement of the Kármán vortex street and the rapidly changing morphologies of the cyclones between August 1994 and October 1996 are illustrated in Fig. 4. In the top frame, the cyclone C4 between the anticyclones WO1 and FA is a long, dark structure with a small, bright spot at the center. The next image, taken 6 months later, shows C4 as a compact, bright ring of clouds with a dark center. The next two images in Fig. 4, taken 8 and 20 months later, show C4 as a wispy cloud with a fuzzy boundary very similar in appearance to C2 and C3 in the four frames.

Small, ephemeral anticyclones have occasionally appeared in the row of white ovals, and they can exist for months or years before they merge with another vortex. An example is WO1, which is visible in the HST image from 21 October 1996 (Fig. 4), but is not visible in the HST image on November 1997 (Fig. 5).

2.4. Merger epoch (1997–2000)

Unfortunately, no images exist of the merger of white ovals BC and DE, but the scenario of events leading to it is the following: by July 1997, ~7 months before merger, the vortices in the Kármán vortex street were strongly interacting with each other. Fig. 6a shows vortices BC and DE on 28 July 1997 with the cyclone C2 between them being squeezed and pulled southward by BC. According to A. Simon (private communication, 1998), 3 or 4 months before the white oval merger (September or October of 1997) there was a merger between FA and WO1, creating the vortex in Fig. 5 labeled FA + WO1. By November 1997, the C4 cyclone was no longer visible (it was last seen in April 1997), and presumably it must have merged with another cyclone or it was destroyed. Simon (private communication, 1998) believes that C3 had disappeared by this time, although we have tentatively identified a dark

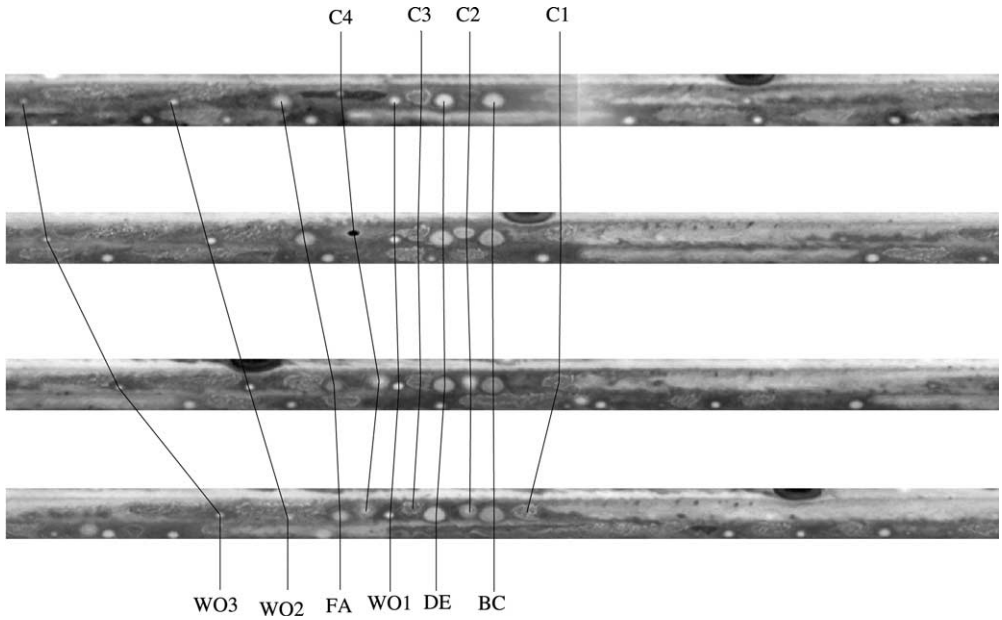

Fig. 4. HST mosaics (Simon et al., 1998) taken (from top to bottom) on 24 August 1994, 17 February 1995, 5 October 1995, and 21 October 1996 showing the white ovals and the cyclonic systems between them. The images are centered at the eastern edge of BC as it traveled around the planet, and they span 360° in longitude.

elliptical region in a November 1997 HST image (Fig. 5) as C3. (see Section 5.) Just prior to the merger, the eastward drift speeds of white ovals FA and DE increased, and the merger occurred in late 1997 or early 1998. Sánchez-Lavega et al. (1999) used ground-based observations to argue that it occurred in February 1998. Simon describes the merger as "cars piling up at a stop light" with BC "slamming on its breaks" and the rest of the vortices forcing DE to merge with BC (press report, K. Chang, October 19, 1998, "Jupiter Storms Collide," ABC-NEWS.com). (Unlike cars, vortices have no inertia—their densities are the same as the ambient fluid—and it is misleading to apply one's intuition about objects with mass to vortices.) Fig. 7 taken in June 1998 shows that BC and DE had merged to become the new vortex BC + DE. It also shows the anticyclone made from FA and WO1, which merged between September and October 1997. Simon (private communication, 1998) believes that the bright elliptical cyclone between FA + WO1 and BC + DE in Fig. 7 is C2 (but we believe it is C2 + C3—see Section 4). White oval FA merged with BC + DE in 2000 (Sánchez-Lavega and colleagues, 2000), although details of the merger and the role of the intervening cyclone have not yet been published. Obviously many questions remain about the sequence of events that led to the merger, including the identifications and positions of some of the surviving vortices. We now turn to theory and numerical simulation to help answer them.

3. Theoretical overview of planetary vortex dynamics

3.1. Assumptions

To understand the white ovals, it is important to review the properties of planetary vortices. We assume that the

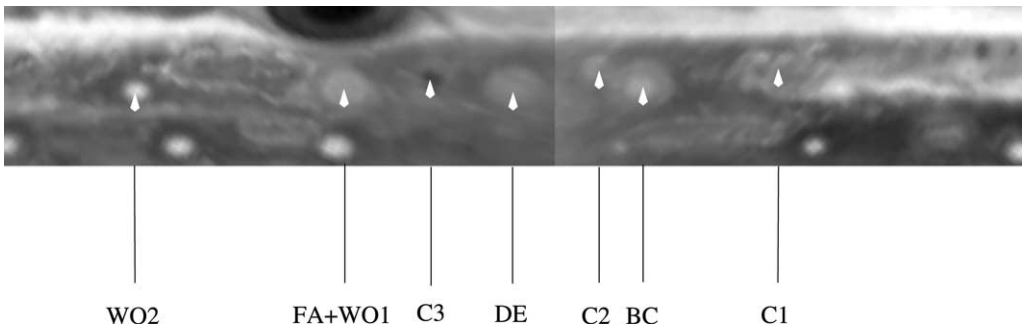

Fig. 5. An HST mosaic (Simon, private communication 1998) taken in November 1997 showing that WO1 was no longer present and (in our opinion) has merged with FA. The identification of the dark region as C3 is tentative. C4, formerly between FA and WO1, is no longer visible.

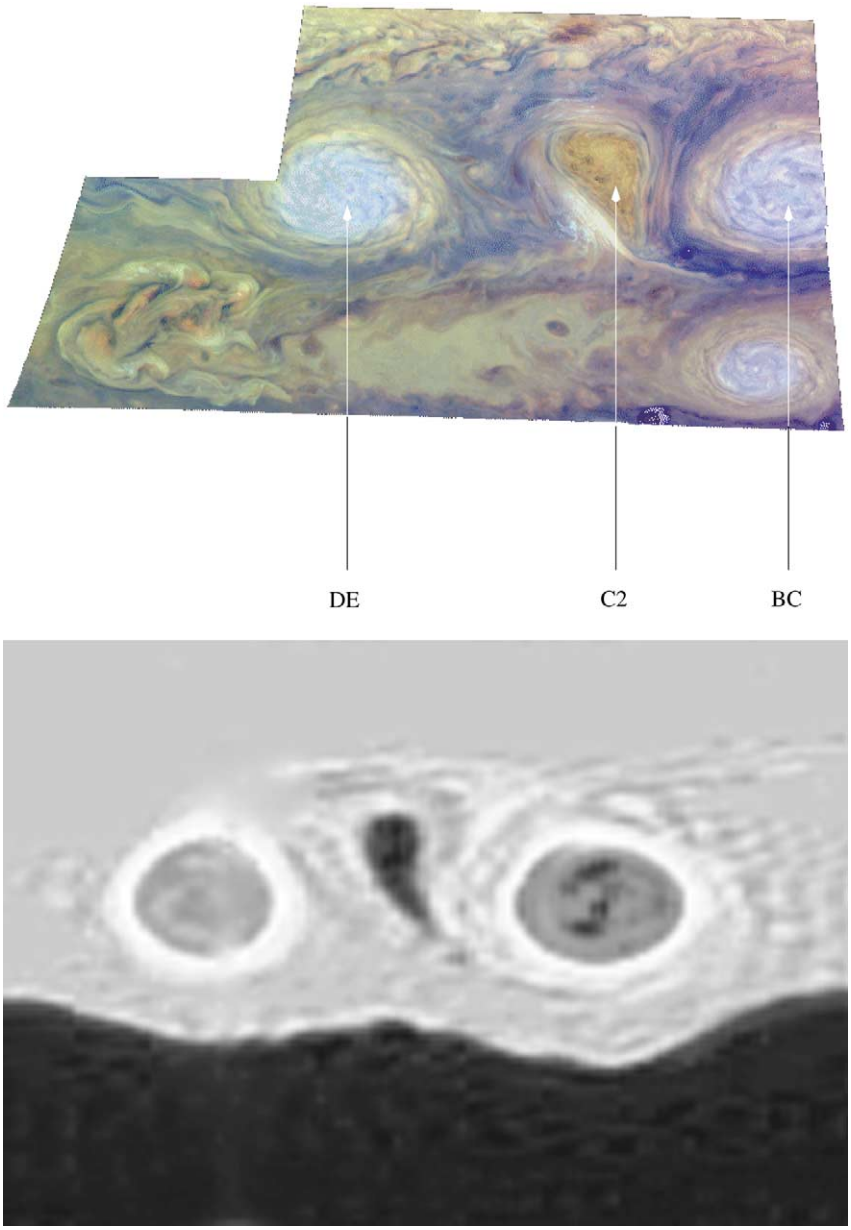

Fig. 6. (top) A *Galileo* spacecraft mosaic (Vasavada et al., 1998) from 28 July 1997 showing cyclone C2 being squeezed between white ovals BC and DE approximately 6 months before the merger of BC and DE. (bottom) Numerical simulation of a cyclone squeezed between two anticyclones. This image is a spatial blow-up of one of the frames, $t = 41$ days, in the numerical calculation illustrated in Fig. 23.

weather layer of atmosphere containing the white ovals obeys the shallow-water (SW) equations (Pedlosky, 1987), although in some cases we further assume they they obey the more restrictive QG equations (Marcus, 1993). We also assume that the vortices are characterized by compact regions of anomalous potential vorticity q (Pedlosky, 1987). Most analyses of jovian vortices have used either the SW (Cho and Polvani, 1996; Kim, 1996) or QG equations (Ingersoll and Cuong, 1981; Marcus, 1988). Dowling and Ingersoll (1988, 1989) used both in analyzing the GRS and found little difference. Because the QG approximation is more easily satisfied for small vortices than it is for large, and more easily for vortices near the pole than the equator, the fact that QG works well for the GRS suggests it should work for the white ovals.

Numerical SW and QG simulations show that flows tend to form regions in which q homogenizes to nearly uniform values with large gradients of q at the interfaces between them (McDowell et al., 1982; Marcus, 1988; Kim, 1996). McDowell et al. noted that this phenomena is also observed in the Earth's atmosphere and oceans. The average q of the jovian atmosphere decreases from the north to south, due to the fact that $f(y)$, the Coriolis parameter, decreases. Simulations of flows with a jovian-like $f(y)$ show homogenization with an additional feature. The regions with near-uniform q align as east–west bands that circumscribe the planet and

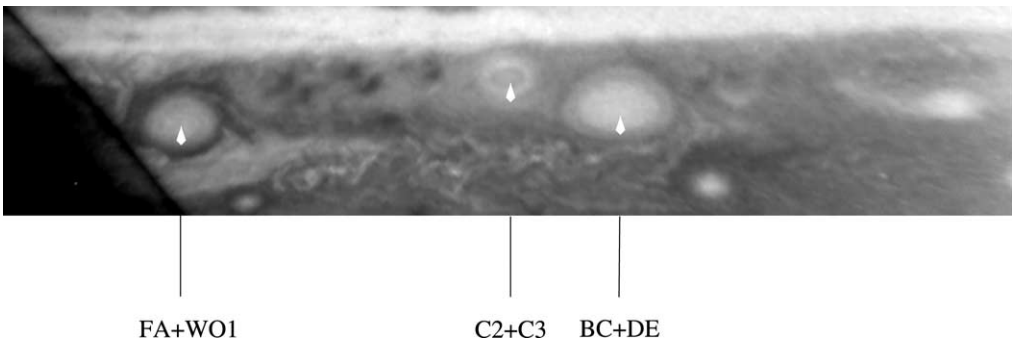

Fig. 7. An HST mosaic (Simon, private communication, 1998) from June 1998 showing the merged vortex BC+DE.

the gradients of q are located at (and create) the eastward jets (Marcus, 1993; Marcus and Lee, 1994; Cho and Polvani, 1996; Marcus et al., 2000). Similar results are seen in laboratory experiments that have a topographically produced β-effect (Sommeria et al., 1989; Solomon et al., 1993). The same simulations and experiments also show robust, compact vortices (characterized by local changes in q) superposed on the bands. Based on these observations, we characterize the q of the jovian weather layer as a step function that decreases from north to south with the steps (discontinuities in q) located at the eastward jets. Between the eastward jets, q is nearly uniform with the exception of the anomalies Δq associated with the vortices.

3.2. Advection of potential vorticity

For both the SW and QG equations, the potential vorticity is advectively conserved, $Dq/Dt = 0$, so if the white ovals are potential vorticity anomalies superposed on an east–west flow with nearly uniform q and if the conditions for the SW approximation hold, then they cannot be destroyed or even decay over time. Instead, they advect with the local velocity, which is the sum of the ambient east–west velocity $u(y)$ (in Fig. 2) and the velocities created by other potential vorticity anomalies. (However individual vortices do not self-advect.) Those anomalies include any nearby vortices as well as the discontinuities in q corresponding to eastward jets. The velocity produced by a vortex is calculated with the Biot–Savart Law with anticyclones creating counterclockwise circumferential flows about their centers and clockwise flows for cyclones. (In this paper we assume a southern hemisphere reference.) The velocities produced by a vortex decrease exponentially away from it with an e-folding length equal to the Rossby deformation radius, so only nearby vortices are relevant for advection.

3.3. Vortices embedded in shearing flows

Numerically it has been shown that both cyclonic and anticyclonic vortices exist in the SW equations. In fact for the QG equations, cyclones and anticyclones behave identically (except the signs of their velocities are reversed). However, when a vortex with a characteristic potential vorticity anomaly Δq is embedded in a flow with shear σ, then the vortices are robust only if Δq and σ have the same sign (or when the zonal shear is very weak, i.e., $|\sigma| \ll |\Delta q|$). When they have opposite sign, the wind rips the vortex apart on a fast, advective timescale (Marcus, 1993). Thus anticyclones are embedded in anticyclonic zones, and cyclones are embedded in cyclonic belts (Marcus, 1990, 1993). This theoretical result is consistent with all catalogued jovian vortices — whether they are identified as robust, ephemeral, or cyclonic filamentary regions (MacLow and Ingersoll, 1986). Eastward and westward jets (i.e., the locations where σ changes sign) can be deflected by vortices. Fig. 8 shows a numerical simulation of a Kármán vortex street (Humphreys, 2000). The westward jet threading between opposite-signed vortices is distorted by the vortices from its usual longitude-independent location. North (south) of the westward jet, both the vortices and the shear due to the east–west wind are cyclonic (anticyclonic). Stronger vortices distort the westward jet even more than in Fig. 8, so the centers of vortices of different sign can be nearly at the same latitude yet lie in shears with the same signs as the vortices. An example of this is the chain of jovian vortices at 41°S latitude (Humphreys, 2000).

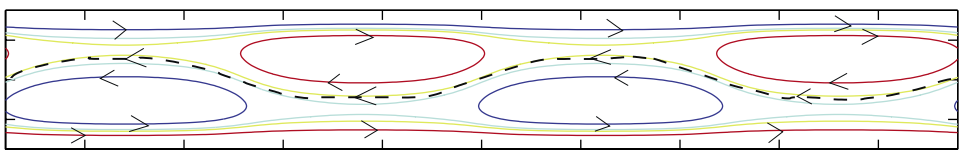

Fig. 8. A numerically computed (using contour dynamics) Kármán vortex street with eastward jets to its north and south. A westward jet, shown as a heavy broken curve, threads between the rows of opposite-signed vortices.

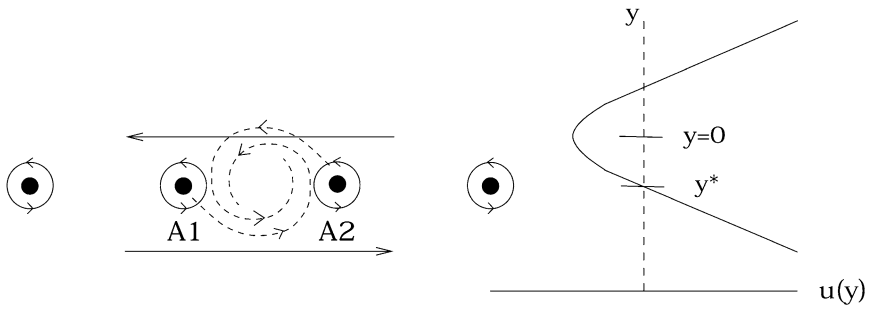

Fig. 9. Four like-signed anticyclones in a row that is unstable to vortex mergers. Solid curves represent fluid flow, and broken curves show the movement of the vortices. The average east–west velocity $u(y)$ with a westward jet at $y = 0$ is also shown.

3.4. Kármán vortex streets

The white ovals are just one example in which two or more long-lived anticyclones coexist at the same latitude. It had been conjectured (Marcus, 1993), and here we show numerically, that one way this can happen is if the vortices are part of a Kármán vortex street. After carrying out many numerical experiments (with the QG and SW equations as well as the full 3D Navier–Stokes equation), we still know of no other way to stabilize a row of like-signed, finite-area vortices. Consider the difficulties. Fig. 9 shows schematically a row of anticyclones embedded in an anticyclonic shearing flow. It can be shown that a steady equilibrium exists only if the vortices all have the same $|\Delta q|$ and area, and are equally separated. In that case, the row is unstable and the vortices approach each other and merge. To see this, choose a reference frame moving with the vortices such that $u(y^*) = 0$ where anticyclones **A1** and **A2** are at latitude y^*. If either small perturbations or the velocities due to the other vortices displace vortex **A2** upward where $u(y) < 0$, then both $u(y)$ and the velocities due to the other vortices cause **A2** to move to the left. The velocity produced by **A2** then causes **A1** to move downward where $u(y) > 0$. The $u(y)$ at this latitude then advects **A1** to the right toward **A2**, which is still moving to the left. In other words, once the two vortices are at different latitudes, the differential velocity of $u(y)$ causes the two vortices to approach each other. Numerical simulations show that when like-signed vortices get within approximately a diameter of each other, they merge within two or three vortex turn-around times (Marcus, 1993).

Now consider the same anticyclones as part of a Kármán vortex street. The staggered cyclones **C1** and **C2** are north of the anticyclones and are embedded in cyclonic shear (Fig. 10). This configuration is stable even if the vortices have different $|\Delta q|$, area, or initial separations. The vortices typically oscillate in longitude while maintaining nearly constant latitude. Like-signed vortices never come close to each other and therefore never merge. To see this, consider vortex **A2** in Fig. 10. If it is perturbed upward, it is pushed to the left by $u(y)$ as before. However, now as it approaches **C1**, it is pushed downward where $u(y)$ pushes it back to the right toward its original location. **A2** is repelled by **C1** and is therefore prevented from getting close to **A1**. An intervening cyclone between two anticyclones prevents them from getting close. The vortices reverse direction when they encounter an opposite-signed vortex from the other row *not a like-signed vortex from their own row.*

Recently, Humphreys has shown that the vortices within a Kármán vortex street slowly evolve over thousands of vortex turn-around times by accreting smaller vortices and shedding filaments (Humphreys, 2000). For a vortex street in which the rows of cyclones and anticyclones are initially far apart in latitude, the two rows move closer together until the westward jet between them is nearly pinched off (Fig. 8), and then they stop moving in latitude. In the southern hemisphere this would be observed as a slow northward drift of a row of anticyclones until their northern edges protrude north of the latitude traditionally associated with the westward jet, the demarcation of the southern side of a belt (or northern side of a zone). This northward drift of the white ovals was observed (Rogers, 1995).

3.5. The repulsion of opposite-sign vortices

The repulsion between opposite-signed vortices straddling a westward jet can be quantified by considering the vortices **C** and **A** in Fig. 11, where **C** is a cyclone and **A** is an anticyclone, with centers of vorticity located at $(x_C(t), y_C(t))$ and $(x_A(t), y_A(t))$, respectively. The vortices have potential circulations $\Gamma_A \equiv \int \Delta q_A \, dxdy$ and $\Gamma_C \equiv \int \Delta q_C dxdy$, where the integrals are taken over the respective

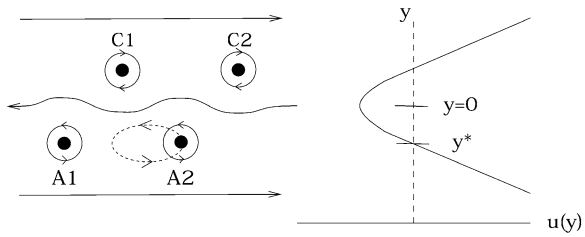

Fig. 10. Vortices in a Kármán street. This configuration is stable to vortex mergers. Solid and broken curves are as described in the legend to Fig. 9.

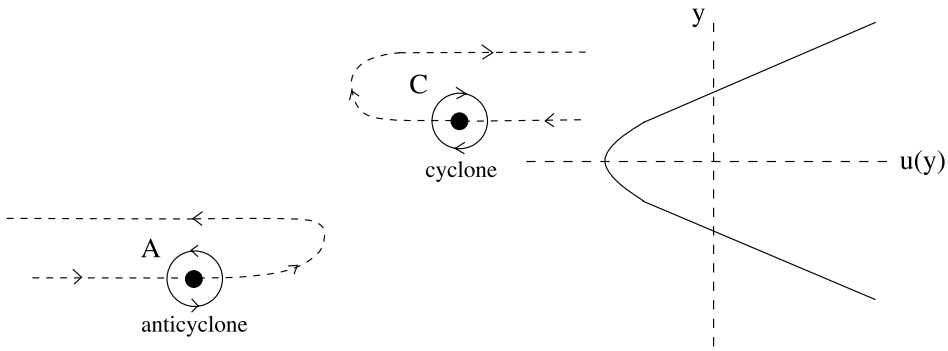

Fig. 11. A schematic showing how anticyclones and cyclones repel when they straddle a westward jet. Solid and broken curves are as described in the legend to Fig. 9.

areas of the vortices. Assuming the absolute value of the longitudinal separation X between the two vortices is large compared to their sizes and to their latitudinal separation, and that the vortices are acted on only by the zonal wind and each other, the mutual acceleration between the two vortices $\ddot{X}$ is approximately

$$\ddot{X} = \frac{|\sigma_A\Gamma_C + \sigma_C\Gamma_A|}{2\pi L_r} K_1(X/L_r), \tag{1}$$

while the acceleration on the anticyclone alone due to the repulsion is

$$|\ddot{x}_A| = \frac{|\sigma_A\Gamma_C|}{2\pi L_r} K_1(X/L_r), \tag{2}$$

where K_m is the modified Bessel function of the second kind of order m (which for $m = 1$ decreases exponentially for large arguments and acts as the inverse of its argument for small arguments) and L_r is the Rossby deformation radius. Eq. (1) shows a repulsion that decreases with distance, quite different from Sato's Hooke's-law inspired fit in Section 2.2, which is between two anticyclones rather than a cyclone/anticyclone pair and which increases rather than decreases with the separation between the vortices.

The integral of Eq. (1) gives the relative velocity V between the anticyclone and cyclone as a function of X: $V \equiv \dot{X}$, where

$$V^2 = \left(\frac{|\sigma_A\Gamma_C + \sigma_C\Gamma_A|}{\pi}\right)\left[K_0\left(\frac{X_{ca}}{L_r}\right) - K_0\left(\frac{X}{L_r}\right)\right]$$
$$= V_\infty^2 - \left(\frac{|\sigma_A\Gamma_C + \sigma_C\Gamma_A|}{\pi}\right)K_0\left(\frac{X}{L_r}\right), \tag{3}$$

where X_{ca} is the value of X at the closest approach between the cyclone and anticyclone, and

$$V_\infty = \pm\sqrt{|\sigma_A\Gamma_C + \sigma_C\Gamma_A|K_0(X_{ca}/L_r)/\pi} \tag{4}$$

is the value of V as X becomes large compared with L_r (both before and after the encounter). K_0 decreases exponentially for large arguments and is proportional to log for small arguments.

As the anticyclone oscillates in longitude between one or more cyclones it makes an elongated counterclockwise orbit with its northern- and southern-most latitudes relatively close together. Similarly, a cyclone follows an elongated clockwise orbit. The shift in latitude of an anticyclone after it is repelled by a cyclone (measured when X/L_r is large before and after the encounter) is

$$|\Delta y_A| = 2|\Gamma_C|\sqrt{K_0(X_{ca}/L_r)/\pi|\sigma_A\Gamma_C + \sigma_C\Gamma_A|}\,, \tag{5}$$

and the change in its velocity $|\Delta v_A|$ is

$$|\Delta v_A| = 2|\sigma_A\Gamma_C V_\infty|/|\sigma_A\Gamma_C + \sigma_C\Gamma_A|$$
$$= 2|\sigma_A\Gamma_C|\sqrt{K_0(X_{ca}/L_r)/\pi|\sigma_A\Gamma_C + \sigma_C\Gamma_A|}\,. \tag{6}$$

The latitude of the anticyclones is more northerly (southerly) after a close approach with a cyclone to its east (west). The distance of closest approach X_{ca} decreases with increasing $|V_\infty|$. Unfortunately, locations of the jovian cyclones are difficult to determine. Neither their locations nor their translational velocities were recorded historically, so the distance of closest approach cannot be determined and used to verify or refute Eqs. (1)–(5). However, X_{ca} may be eliminated from Eqs. (1)–(6) to obtain equations for quantities that have been observed and recorded,

$$|\Delta y_A| = |\Delta v_A/\sigma_A| \tag{7}$$

and

$$|\ddot{x}_A|_{max} = |\sigma_A|(\Delta y_A)^2|\sigma_A\Gamma_C + \sigma_C\Gamma_A|/8L_r|\Gamma_C|\,, \tag{8}$$

where $|\ddot{x}_A|_{max}$ is the maximum east–west acceleration of an anticyclone during a repulsion (which occurs at closest approach).

3.6. Rossby wave trapping

The repulsion mechanism in the proceeding section shows that neither a Kármán vortex street nor a fragment of it could, in general, be confined in a tight packet. An initially tight packet of vortices will spread apart, moving its end vortices outward with a velocity

$$\sqrt{|\sigma_A\Gamma_C + \sigma_C\Gamma_A|K_0(S/L_r)/\pi}\,, \tag{9}$$

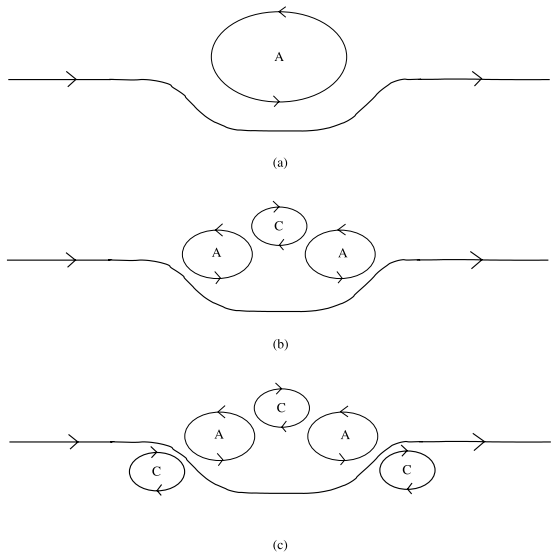

Fig. 12. (a) Schematic of an anticyclone trapped in the trough of a Rossby wave. The eastward jet south of the anticyclone is associated with a jump in q of strength ΔQ_{jet}. The flow south of the jet is more cyclonic. (b) Same as (a) but with three trapped vortices. (c) Same as (b) but with the cyclonic flow making up the two sides of the trough replaced by virtual cyclones.

where S is the distance between the end vortex and its nearest neighbor. We now report a new mechanism that prevents spreading and confines a Kármán vortex street. As discussed in Section 3.1 the eastward jets are associated with discontinuities of q. A discontinuity of strength ΔQ_{jet} supports a Rossby wave. We reported previously that a Rossby wave can trap a vortex so that the vortex is carried along at the same speed as the wave (Marcus and Lee, 1994). This is schematically shown in Fig. 12a, which shows a vortex lying in the trough of a Rossby wave, which is guided along the deformed eastward jet (i.e., the locus of the discontinuity ΔQ_{jet}). Our numerical calculations showed that the Rossby wave trapping was robust with respect to large perturbations. The same trapping phenomena have also been observed in laboratory experiments (Sommeria et al., 1989). Rossby-wave trapping can be understood by examining the schematic in Fig. 12. The flow south of the eastward jet is more cyclonic than that to the north. Part of the advection of the anticyclone is due to the ΔQ_{jet} of the eastward jet, and it is this part that traps the vortex. The two sides of the Rossby wave's trough (to the immediate east and west of the anticyclone and just south of the eastward jet) contain flow that is more cyclonic than the flow immediately surrounding the anticyclone. To see the trough's effect, we replace its two sides with two virtual cyclones as in Fig. 12c. Using the repulsion mechanism discussed in the previous section, we see that if the two virtual cyclones were constrained to remain a fixed distance apart from each other, then an anticyclone between them would be trapped, oscillating back and forth between them but not escaping. A Rossby wave on an eastward jet can trap more than one vortex. It can trap a Kármán vortex street with any odd number of vortices (Fig. 12c). If the street is on the northern (southern) side of the Rossby wave, then the two end vortices must be anticyclones (cyclones).

4. Numerical illustrations of planetary vortex dynamics

To illustrate the trapping and merger of vortices we carried out several dozen numerical calculations. Typical examples are shown in Figs. 21–23. (The descriptions of these particular simulations are in Section 5.3.) They were computed using the QG equations solved with a high-resolution spectral code whose details have been described elsewhere (Marcus and Lee, 1994). From these simulations we were able to examine the individual steps needed to allow vortex mergers under the unusual condition that the vortices were initially members of a Kármán vortex street embedded in a shearing zonal flow.

4.1. Hops as a prelude to merger

It would appear that Kármán vortex streets are so stable, and the cyclone/anticyclone repulsion so strong that the vortices in the street never merge. However, if a cyclone and an adjacent anticyclone were to exchange longitudinal locations in a street by "hopping" over each other, then a pair of cyclones would be adjacent with no intervening anticyclone, and a pair of anticyclones would be adjacent with no intervening cyclone. The two anticyclones would then approach and merge on an advective timescale, as would the two cyclones. (The advective timescale is $\Delta x/\sigma\Delta y$, where σ is the ambient shear, Δx is the longitudinal separation between the adjacent, like-signed vortices, and Δy is their latitudinal separation.) In all of our numerical simulations of Kármán vortex streets we found that mergers come in pairs—two anticyclones merge and two cyclones merge—and that mergers are preceded by a "hop." This observation has allowed us to determine the prerequisites for a merger by computing the necessary conditions for a hop. Eq. (1) shows that the cyclone/anticyclone repulsion mechanism requires that the vortices be embedded in shear flow; if the shear is sufficiently small, or equivalently if the approach velocity of the two vortices V_∞ is sufficiently large, then the repulsion can be overcome and the vortices hop. Numerically we have shown that for vortices with potential circulations and ambient shears like the white ovals and their associated cyclones, a hop occurs if the distance of closest approach X_{ca} between a cyclone and an anticyclone is less than $\sim 3L_r$. When vortices come this close, they exert tides on each other, distort, and slide past one another. Requiring that $X_{\text{ca}} \leq 3L_r$, Eq. (4) shows that a hop occurs when

$$u(y_{\text{C}}) - u(y_{\text{A}}) = V_\infty \geq [|\sigma_{\text{A}}\Gamma_{\text{C}} + \sigma_{\text{C}}\Gamma_{\text{A}}|K_0(3)/\pi]^{1/2} \qquad (10)$$

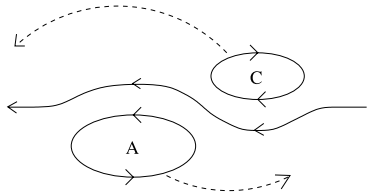

Fig. 13. Preferred 2-body counterclockwise hop.

or equivalently, using Eq. (6)

$$\Delta v_A \geq 2|\sigma_A\Gamma_C|\,[K_0(3)/\pi|\sigma_A\Gamma_C + \sigma_C\Gamma_A|]^{1/2}, \quad (11)$$

where y_A and y_C are the vortex latitudes when they are far from each other. Eq. (11) means that we would not expect to see an anticyclone reverse direction with a velocity change that satisfies the inequality; instead, the anticyclone would hop over the cyclone rather than be repelled by it.

The analysis leading to Eqs. (1)–(4) and Eqs. (10) and (11) includes only the leading-order terms. The next-order correction, which takes into account the finite area of the vortices, shows that the two types of hops shown in Figs. 13 and 14 are not equivalent. The self-advection of a cyclone/anticyclone pair (calculated with the Biot–Savart law) both translates and rotates it. The direction of rotation has the same sign as the vortex with the larger potential circulation. The white ovals have larger circulations than their associated cyclones (see Appendix B), so the self-advection of the cyclone/anticyclone pair tries to rotate it counterclockwise about its geometric center. The counterclockwise hop in Fig. 13, where the cyclone approaches the anticyclone from the east and passes westward to the north of it, is aided by the self-advection, while the clockwise hop in Fig. 14 is inhibited. If a 2-body hop were to occur in the Kármán vortex street containing the white ovals, we would expect it to be counterclockwise.

Using Eqs. (10) and (11) and our best estimates (see Appendix B) for the circulations of the white ovals BC and DE and of the intervening cyclone C2, for C2 to hop DE and allow the merger of BC and DE, requires $V_\infty > 30$ ms^{-1}, or $\Delta v_A > 3.0$ ms^{-1}, or $(y_C - y_A) > 2000$ km. This is confirmed by a series of numerical experiments in which an anticyclone and a cyclone were initially placed close to each other in latitude but separated by several L_r in longitude. Due to the shear of the average jovian east–west velocity $u(y)$ (Fig. 2) the vortices initially approach each other with velocity V_∞. Table 1 along with Fig. 19 summarizes experiments in which V_∞ and the circulations of the vortices were varied. The table was compiled using our best estimate (see Appendix B) of the circulations in the white ovals. Table 2 is similar to Table 1 but uses a smaller value of circulation. The hop looks qualitatively like that shown in the fourth frame of Fig. 23 and Fig. 13. The numerical experiments also show that the nonpreferred hop in Fig. 14 requires a value of V_∞ approximately 15% larger than the preferred hop. Therefore, there is a range of values of V_∞ for which a cyclone approaches an anticyclone from the east, is repelled by it, travels around the planet, reapproaches the anticyclone (or another anticyclone in the vortex street) from the west (the preferred hop direction), and then hops.

The 2-vortex hop calculations summarized in Figs. 19 and 20 show that even for the smallest plausible values of the circulations of the cyclones (see Appendix B), the observed approach speeds and latitudinal separations of the

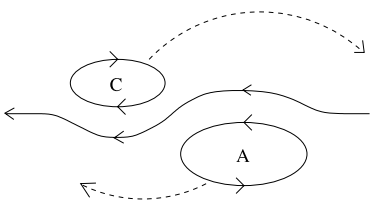

Fig. 14. Nonpreferred, 2-body clockwise hop.

Table 1
Two-vortex interactions computed with $\Gamma_A = 5.0 \times 10^3$ km^2/s^{-1}

AC position (°S)	Δb	V_∞ (m/s)	Γ_C/Γ_A					
			0.05	0.10	0.15	0.20	0.25	0.50
34.60	3000 km ~ 2.60°	19.5	R	R	R	R	R	R
35.11	3600 km ~ 3.11°	25.9	F	F	R	R	R	R
35.24	3750 km ~ 3.24°	27.7	FH	F	F	F	FR	R
35.37	3900 km ~ 3.37°	29.4	H	H	H	H	H	R
35.63	4200 km ~ 3.63°	33.4	H	H	H	H	H	R
35.88	4500 km ~ 3.88°	38.7	H	H	H	H	H	H
36.14	4800 km ~ 4.14°	43.4	H	H	H	H	H	H

Note. The initial vortices have nearly uniform value of q with $q_A = 1.1 \times 10^{-4}$ s^{-1} and $q_C = 4.7 \times 10^{-5}$ s^{-1}. These are our best estimates of the jovian values. The initial shapes of the vortices are that of isolated equilibria. The vortices are embedded in the shearing flow $u(y)$ shown in Fig. 2. The first column shows the initial latitude y_A of the anticyclone. The second shows that of the (more northern) cyclone with $y_C = y_A - \Delta b$. $V_\infty = u(y_A) - u(y_C)$. The value of Γ_C/Γ_A was changed in each numerical experiment by adjusting the initial value of the cyclone's area. The result of each experiment is labeled with: R, indicating that the vortices repelled rather than hopped; H, indicating that they hopped; FH, indicating that the vortices collided, fractured into several pieces and that most of the pieces hopped; or FR, indicating that they fractured and that most of the pieces repelled. In Tables 1–6, y_C is at 32°S.

Table 2
Two-vortex interactions with all parameters the same as in Table 1 but with smaller area anticyclones such that $\Gamma_A = 6.3 \times 10^2$ km^2 s^{-1}

AC position (°S)	Δb	V_∞ (m/s)	Γ_C/Γ_A					
			0.05	0.10	0.15	0.20	0.25	0.50
34.60	3000 km ~ 2.60°	19.5	R	R	R	R	R	R
35.11	3600 km ~ 3.11°	25.9	H	H	R	R	R	R
35.24	3750 km ~ 3.24°	27.7	H	H	H	H	H	R
35.37	3900 km ~ 3.37°	29.4	H	H	H	H	H	R
35.63	4200 km ~ 3.63°	33.4	H	H	H	H	H	H
35.88	4500 km ~ 3.88°	38.7	H	H	H	H	H	H
36.14	4800 km ~ 4.14°	43.4	H	H	H	H	H	H

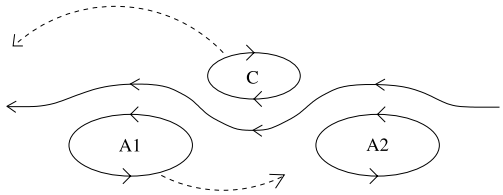

Fig. 15. Preferred, 3-body counterclockwise hop of a central cyclone. The "hopping" vortices are denoted with long dashed arrows.

white ovals, $\Delta v_A \leq 1$ ms^{-1} and $(y_C - y_A) < 1000$ km, were far too small to hop by the theoretical and numerical criteria listed above. We know of no atmospheric event that could perturb the atmosphere with such violence that it would satisfy these criteria. For example, the Shoemaker–Levy comet impact caused no observable changes in either the velocities or positions of the vortices in the weather layer.

Due to the implausibility of a 2-body hop, we consider next the four types of 3-body hops shown schematically in Figs. 15–18. An analytic expression for the necessary conditions for a 3-body hop is complicated and not very illuminating. Instead, we present heuristic arguments and summarize our numerical experiments. Assuming that the anticyclones have larger potential circulations $|\Gamma_A|$ than the cyclones $|\Gamma_C|$, the hops in Figs. 15 and 18 are preferred (i.e., require less V_∞) to those in Figs. 16 and 17 because the hopping cyclone/anticyclone pairs in the preferred cases rotate counterclockwise like the anticyclones. To see that the hop in Fig. 15 is preferred over the hop in Fig. 18, consider the role of the third, "nonhopping" vortex, and assume it primarily affects only its nearer neighbor because its influence decreases exponentially at distances greater than L_r. In Fig. 15 the velocity created by the nonhopping vortex A2 pushes the adjacent cyclone C to the west, which facilitates the hop. Secondly, and more importantly (as we can show numerically) A2 pushes C to the south toward the westward jet where the ambient $u(y)$ becomes more westward and further pushes C to the west. The latter contribution to the westward velocity of C is proportional to $|\sigma_C \Gamma_A|$. In Fig. 18 the velocity created by the nonhopping vortex C1 pushes the adjacent anticyclone A to the west, which inhibits its hop around C2. C1 also pushes A to the south where the ambient $u(y)$ becomes more eastward and helps push A to the east, facilitating the hop. However, this eastward push is small (compared to the westward push from the nonhopping vortex in Fig. 18) because it is proportional to $|\sigma_A \Gamma_C|$.

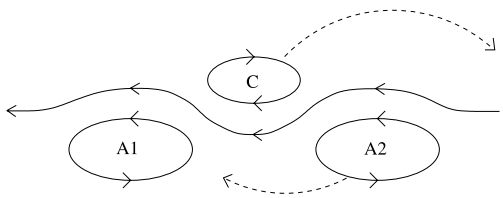

Fig. 16. Three-body clockwise hop of a central cyclone.

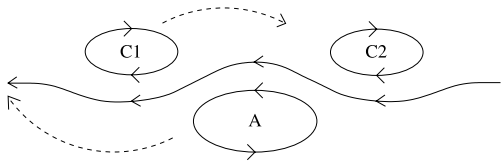

Fig. 17. Three-body clockwise hop of a central anticyclone.

Thus, for the white ovals, we would expect that the hop in Fig. 15 is preferred and requires a smaller V_∞ than any of the other 3- or 2-body hops. The numerical experiments summarized in Tables 3 and 4 confirm these heuristic arguments.

It might be argued that it would be unlikely that three vortices would all approach each other simultaneously and therefore unlikely 3-body hops on Jupiter would occur. However, if three or more vortices are trapped in a single Rossby wave trough, then there are many opportunities for 3-body hops. Moreover, as we show below, the sides of the trough squeeze the 3 vortices together and lower significantly the required V_∞ needed for a hop.

We carried out numerical experiments to determine the critical, minimum values of V_∞ needed for a 3-body hop with the vortices trapped in a Rossby wave. The results are summarized in Tables 5 and 6 and Figs. 19 and 20 . For the figures and Tables 3 and 5, $\Gamma_A = 5.0 \times 10^3$km^2 s^{-1}. For calculations that included a Rossby wave along the eastward jet, we set $\Delta Q_{jet} = 3.9 \times 10^{-5}$ s^{-1}. These values are based on our best estimates of the jovian values. (See Appendix B.) In Fig. 19, the initial areas of the anticyclones and cyclones were 4.5×10^7 and 8.2×10^6 km^2, respectively. These are our best estimates for the white ovals and the intervening cyclones. The initial latitude of the anticyclones were chosen to be their observed locations. The observed latitudes of the cyclones are somewhat uncertain because their clouds do not necessarily correspond to the location of their q anomalies (see Appendix A). Their initial locations are always near their approximate observed locations, but their precise values y_C are input parameters into our calculations. The initial values of y_C determine the initial values of $[u(y_A) - u(y_C)]$. We start with vortices sufficiently separated in longitude so that V_∞ is nearly the same as $[u(y_A - u(y_C)]$. In fact, the values of V_∞ used in Fig. 19 are the initial values of $[u(y_A - u(y_C)]$. In the 3-body numerical experiments, the two anticyclones were initially 20,000 km or $\sim 11 L_r$ apart in longitude, which is approximately equal to the separation between BC and DE in August 1997. The

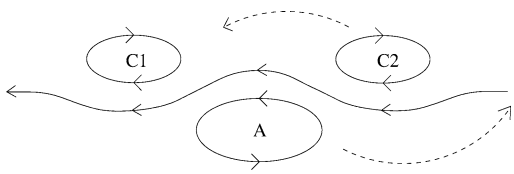

Fig. 18. Three-body counterclockwise hop of a central anticyclone.

Table 3
Three-vortex interactions with same parameters as in Table 1

AC position (°S)	Δb	V_∞ (m/s)	Γ_C/Γ_A					
			0.05	0.10	0.15	0.20	0.25	0.50
34.10	2400 km ∼ 2.10°	13.8	R	R	R	R	R	R
34.60	3000 km ∼ 2.60°	19.5	FH	FR	R	R	R	R
35.11	3600 km ∼ 3.11°	25.9	FH	H	H	H	H	R
35.24	3750 km ∼ 3.24°	27.7	H	H	H	H	H	R
35.37	3900 km ∼ 3.37°	29.4	H	H	H	H	H	R
35.63	4200 km ∼ 3.63°	33.4	H	H	H	H	H	H
35.88	4500 km ∼ 3.88°	38.7	H	H	H	H	H	H

Note. Both anticyclones initially have the same q, circulation, latitude, and shape.

cyclone in our 3-body calculations was initially longitudinally centered between the anticyclones. Like the 2-body hop calculations, the initial positions of the vortices are sufficiently far apart that V_∞ is well approximated by the initial value of $|u(y_A) - u(y_C)|$.

Using a QG, initial-value code (Marcus, 1990) we determined whether a specified initial condition led to hopping or repulsion as a function of Γ_C. Because the value of Γ_C is difficult to determine from the observations, we shall use Figs. 19 and 20 to help establish its value. Fig. 20 is the same as Fig. 19, with the exception that it was computed with vortices with smaller areas (5.7×10^6 km$^2 \cong 2L_r^2$) for both the cyclones and anticyclones and with the same circulations as in Fig. 19. Figs. 19 and 20 were computed with the "preferred" 2- and 3-body hops (i.e., those in Figs. 13 and 15). An example of one of our numerically computed, "preferred," 3-body hops is illustrated in Fig. 23.

Several things can be learned from Figs. 19 and 20. Most importantly, they show that a trapping Rossby wave greatly reduces the V_∞ needed for a hop. Typically, the closing velocity between the intervening cyclones and the white ovals has been less than 1 ms^{-1} during the Kármán Vortex Street and Pre-merger Epochs (1941–1997). Fig. 19 shows that without a trapping Rossby wave, the required V_∞ is too high to allow the merger. Secondly, they confirm our heuristic arguments that the preferred 3-body hop requires less

Table 4
Three-vortex interactions as in Table 3, but with the initial circulations of the anticyclones as in Table 2

AC position (°S)	Δb	V_∞ (m/s)	Γ_C/Γ_A					
			0.05	0.10	0.15	0.20	0.25	0.50
34.60	3000 km ∼ 2.60°	19.5	R	R	R	R	R	R
34.85	3300 km ∼ 2.85°	22.5	FH	R	R	R	R	R
34.98	3450 km ∼ 2.98°	24.1	H	H	H	R	R	R
35.11	3600 km ∼ 3.11°	25.9	H	H	H	H	H	R
35.24	3750 km ∼ 3.24°	27.7	H	H	H	H	H	R
35.37	3900 km ∼ 3.37°	29.4	H	H	H	H	H	R
35.63	4200 km ∼ 3.63°	33.4	H	H	H	H	H	H
35.88	4500 km ∼ 3.88°	38.7	H	H	H	H	H	H

Table 5
Interactions of three vortices trapped in a Rossby Wave

AC position (°S)	Δb	V_∞ (m/s)	Γ_C/Γ_A					
			0.05	0.10	0.15	0.20	0.25	0.50
33.04	1200 km ∼ 1.04°	−1.7	H	R	R	R	R	R
33.56	1800 km ∼ 1.56°	6.7	H	R	R	R	R	R
34.10	2400 km ∼ 2.10°	13.8	H	H	R	R	R	R
34.60	3000 km ∼ 2.60°	19.5	H	H	H	R	R	R
35.11	3600 km ∼ 3.11°	25.9	H	H	H	H	R	R
35.24	3750 km ∼ 3.24°	27.7	H	H	H	H	R	R
35.37	3900 km ∼ 3.37°	29.4	H	H	H	H	H	R
35.63	4200 km ∼ 3.63°	33.4	H	H	H	H	H	R
35.88	4500 km ∼ 3.88°	38.7	H	H	H	H	H	R
36.14	4800 km ∼ 4.14°	43.4	H	H	H	H	H	R

Note. The initial conditions are the same as in Table 3. The Rossby wave has a $\Delta Q_{jet} = 3.9 \times 10^{-5}$ s^{-1}, our best estimate of the jovian value. The flow is as described in the legend to Fig. 22.

V_∞ than the preferred 2-body hop. Thirdly, a comparison of Figs. 19 and 20 shows that the values of the vortex areas have almost no effect and that the important parameters for determining whether vortices repel or hop are Γ_C and the presence of a confining Rossby wave. Fourthly, the critical value of V_∞ for the preferred 2-body hop was well predicted by Eq. (4), with V_∞ increasing with Γ_C.

The fact that the left-hand endpoints of the solid curves in Figs. 19 and 20 do not extend to $\Gamma_C/\Gamma_A = 0$ is indicative that if the circulation of the intervening vortex is too small, the noise in the numerical calculation is sufficient to allow the vortices to hop and merge without supplying an initial approach velocity of the vortices. The right-hand endpoints of the solid curves show that if the circulation of the intervening vortex is too large ($\Gamma_C/\Gamma_A > (\Gamma_C/\Gamma_A)_{crit} \simeq 0.26$) it pushes the two anticyclones apart with such violence that they escape the Rossby-wave trap. If the three vortices are initially close together, but initially untrapped and the circulation of the intervening cyclone decays by ∼10% below $(\Gamma_C/\Gamma_A)_{crit}$, the vortices become trapped. However, these dynamics are outside the scope of this paper.

5. Application of theory to the observations

Here, we will use results from previous sections to explain the white ovals' behaviors during their last three epochs. The physics during the Formation Epoch were probably ageostrophic, and therefore not explainable using our nearly geostrophic (SW or QG) models.

As must be obvious to the reader, we need cyclones to explain the dynamics of the anticyclones. As stated in our Introduction, the consensus opinion is that cyclones are neither long-lived nor coherent. In Appendix A we outline why we think they are both. While the longevity of cyclones is not essential to our explanation of the dynamics of the white ovals, the alternative is less appealing. We would

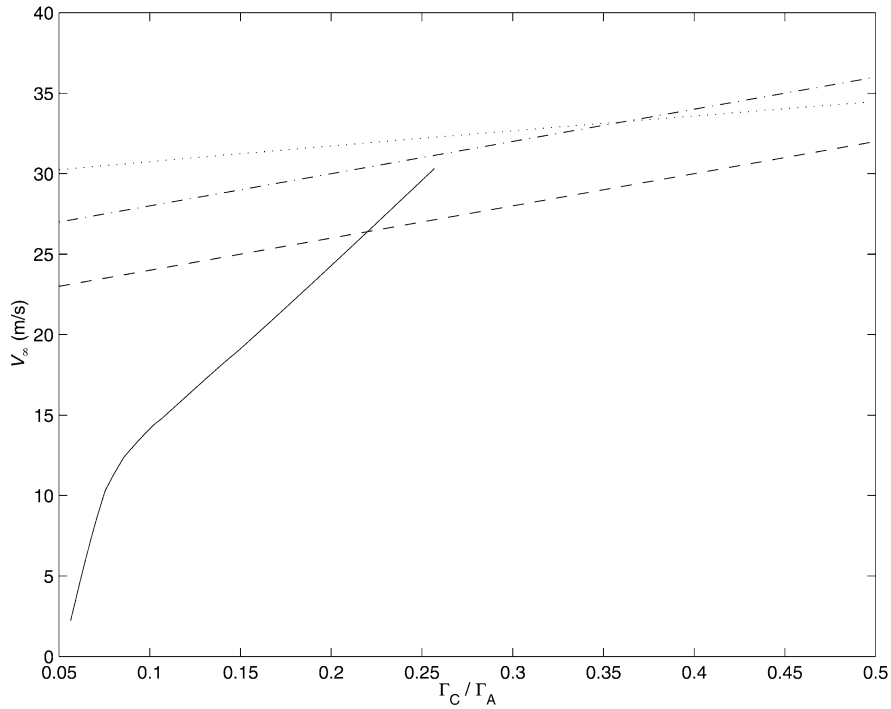

Fig. 19. The critical value of V_∞ above which vortices will hop over each other rather than repel. The dotted line is the theoretical curve based on Eq. (10), the dotted–dashed curve is from the simulations of 2-body hops, the dashed curve of 3-body hops, and the solid curve of 3-body hops with Rossby wave trapping. When Γ_C/Γ_A is greater than the value at the right-hand endpoint of the solid curve, the vortices escape from the Rossby wave trough; when it is less than the left-hand endpoint, our simulations show that the vortices always hop and the anticyclones merge.

require that over the past 60 years, short-lived cyclones just happened to be present each time a pair of anticyclones appeared to repel each other, each time that a pair got close to each other and might have merged, and each time there were satellite observations of Jupiter. (Satellite images have enough resolution to reveal the velocity fields. No satellite image has failed to reveal that the white ovals are staggered with cyclones.)

We remind the reader that there have been many observations of jovian cyclones. For example during the *Voyager* fly-by, there were 12 anticyclones in a row at 41°S, and between almost all pairs there was a "filamentary region" of clouds that was associated with cyclonic flow. The anticyclones were classified as long-lived, while the cyclones were not. Here, as in in most cases, the classification of a jovian vortex as short- or long-lived was based on cloud morphology and color, rather than on a direct observation of the velocity. We believe that this classification is incorrect and that using clouds as indicators of the dynamics is risky. Currently, there are 6 anticyclones at 41°S staggered with 6 "filamentary regions." We see no reason to classify the cyclones as any less coherent or long-lived as the anticyclones—either at 41°S or at latitudes near the white ovals. We believe that coherent cyclones have lifetimes much longer than the color and morphologies of their associated clouds. We now show that these cyclones have a key role in controlling the dynamics of the white ovals.

5.1. Kármán vortex street epoch (1941–1994)

Between 1941 and 1994 we believe the three white ovals were the southern row of a Kármán vortex street. Their northern, cyclonic counterparts were visible during the *Voyager* fly-by as elongated clouds with scalloped edges. The vortices straddled a westward jet so that the the cyclones (anticyclones) were embedded in an ambient cyclonic (anticyclonic) zonal wind. Over this 50-year period the white ovals drifted northward $\sim 2°$, which is consistent with the findings of Humphreys who found that a Kármán vortex street with an initially wide separation between the rows slowly narrows the separation (Humphreys, 2000). The observed, average eastward drift speed of the white ovals also changed during this time. We have argued that, with the exceptions of encounters with cyclones, the white ovals drift with the ambient $u(y)$. This is consistent with observations; moreover, this implies that the ratio of the change in drift speed to the change in latitude of a white oval should be equal to du/dy. The former value is $-1.0 \times 10^{-5}\ \mathrm{s}^{-1}$ (based on Figs. 11.10, 11.11, and 11.16 in Rogers 1995), while the latter was $-1.1 \times 10^{-5}\ \mathrm{s}^{-1}$ at the latitude of the white ovals at the time of the *Voyager* fly-by. This shows that the white ovals drift at the velocity of the local zonal velocity in accord with QG and SW theory (and in dis-

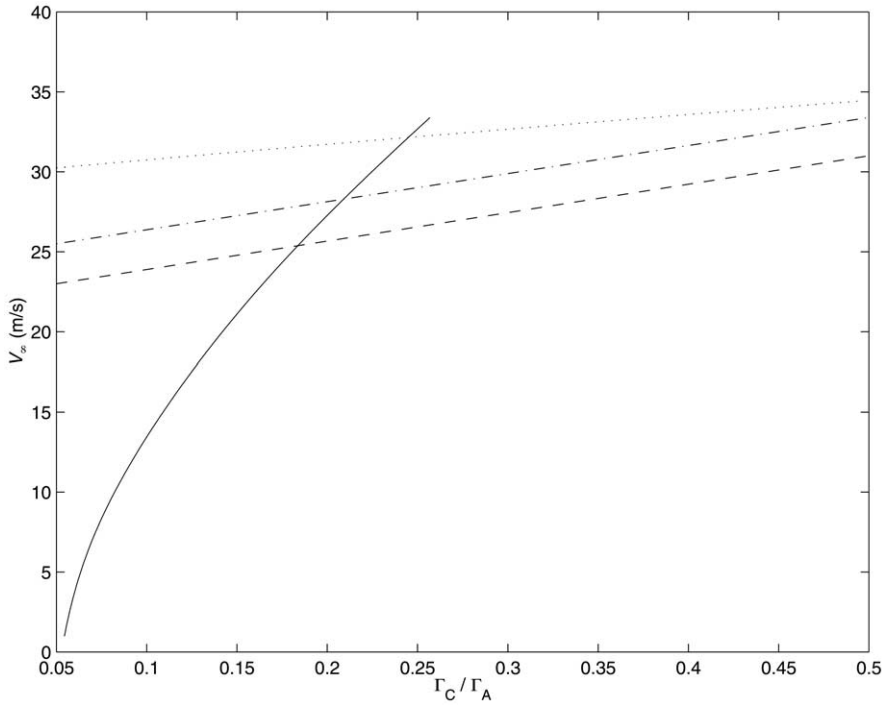

Fig. 20. Same as described in the legend to Fig. 19, but with small-area vortices. See Section 4.1 for details.

agreement with other approximations, such as the intermediate geostrophic equations).

During this epoch, the white ovals approached each other with closing velocities Δv_A of $\sim$1.0 m s^{-1}. (For widely separated vortices, if Δy_A is due to the differential velocity in $u(y)$, then the typical difference in latitudes of the white ovals is $\sim$0.06°.) Based on this closing velocity, if the cyclones had not been present during this time, the white ovals would have encountered each other and merged into a single vortex in only four years. Moreover, the observed values of the relative velocities between the white ovals, $\Delta v_A \simeq 1.0$ m s^{-1}, agree with our picture in two ways. First, they are sufficiently small that according to Fig. 19, the cyclones repel the white ovals rather than allowing them to hop over them and merge. Secondly, the value of Δy_A is accurately predicted by Eq. (5) based on the observed values of the cyclonic circulation Γ_C (see Appendix B).

Table 6
Interactions of three vortices trapped in a Rossby Wave as in Table 5, but with the initial circulations of the anticyclones as in Tables 2 and 4

AC position (°S)	Δb	V_∞ (m/s)	Γ_C/Γ_A					
			0.05	0.10	0.15	0.20	0.25	0.50
33.04	1200 km $\sim$ 1.04°	−1.7	H	R	R	R	R	R
33.56	1800 km $\sim$ 1.56°	6.7	H	R	R	R	R	R
34.10	2400 km $\sim$ 2.10°	13.8	H	H	R	R	R	R
34.60	3000 km $\sim$ 2.60°	19.5	H	H	H	R	R	R
35.11	3600 km $\sim$ 3.11°	25.9	H	H	H	H	R	R
35.24	3750 km $\sim$ 3.24°	27.7	H	H	H	H	R	R
35.37	3900 km $\sim$ 3.37°	29.4	H	H	H	H	R	R
35.63	4200 km $\sim$ 3.63°	33.4	H	H	H	H	H	R
35.88	4500 km $\sim$ 3.88°	38.7	H	H	H	H	H	R
36.14	4800 km $\sim$ 4.14°	43.4	H	H	H	H	H	R

Jovian observations in (Rogers, 1995) show that the relative velocities between white ovals changed signs (i.e., the ovals "repelled" each other) on a number of occasions and that for many of them, the white ovals were more than 10,000 km ($5L_r$) apart. What physics other than an encounter with an unseen or unreported cyclone could cause the mutual velocities between widely separated pairs of white ovals to suddenly change sign? Since the velocity of a vortex falls off exponentially with *e*-folding length L_r, it is difficult to imagine the repulsion was due to an interaction between the white ovals.

Moreover, the values of the accelerations $\ddot{x}_A$ between the white ovals (from Fig. 1.10 in Rogers, 1995) is $\sim 1.3 \times 10^{-5}$ m s^{-2}, which is consistent with our predicted values from Eq. (8) based on the observed values of Γ_C.

5.2. Pre-merger epoch (1994–1997)

In late 1995, the white ovals were traveling together in a tightly spaced group. If this fragment of a Kármán vortex street had not been confined by a Rossby wave (or other mechanism), Eq. (9) shows that the vortices would have spread apart with speed $\sim$1 m s^{-1}, meaning that the longitudinal separation between adjacent white ovals would double in two years. In our simulations, the only way that we have been able to keep a a tightly spaced group of vortices

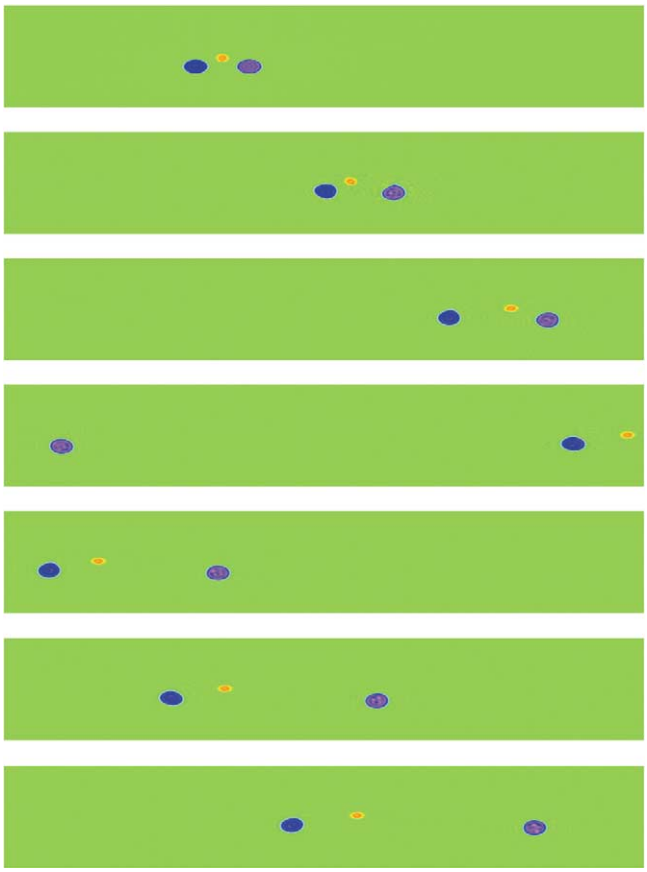

Fig. 21. The potential vorticity q of a fragment of a Kármán vortex street. The eastward jet artificially has $\Delta Q_{\rm jet} = 0$, so it has no Rossby wave. From top to bottom, the frames correspond to $t = 0$, 25, 50, 75, 100, 125, and 150 days. The 3 vortices spread apart with the speed predicted by Eq. (9). A red-to-violet color map is used with red as the most cyclonic and violet as the most anticyclonic.

together is by utilizing the Rossby wave trapping described in Section 3.6. This is a credible mechanism on Jupiter because the eastward jet centered at 36.5°S clearly deforms around the southern side of the Kármán vortex street fragment in Figs. 3–6, cradling it in a trough of a Rossby wave.

In our simulations of Kármán vortex street fragments (Figs. 21–23), we began with 3 vortices superposed on the velocity in Fig. 2. Far from the fragment, the eastward jet was located at its latitude of 36.5°S. Closer to the fragment, the jet was deformed to pass just south of it. The magnitudes of $\Delta Q_{\rm jet}$ the initial areas, q, and circulations of the white ovals $\Delta q_{\rm BC} = 1.1 \times 10^{-4}\ {\rm s}^{-1}$ were set as in Fig. 19, and the initial latitudes and longitudinal separation of the anticyclones were set to their observed values in Fig. 4. The areas, circulations, and latitudes of the jovian cyclones are more difficult to measure, so we initialized our simulation using the indirect methods described in Appendix B. In order to demonstrate the Rossby wave trapping of the white ovals, we used a simplified flow with only two anticyclones and one cyclone rather than trying to simulate the entire chain of vortices shown in Fig. 4. We believe this adequately illustrates the physics without unneeded complication. Fig. 21 shows a time sequence where the entire flow, including both the vortices and the eastward jet, are computed with the QG equations. However, in this calculation we artificially set the $\Delta Q_{\rm jet}$ of the eastward jet equal to 0, so that there was no Rossby wave. The three vortices do not remain confined and spread apart at $\sim$1 m s^{-1} as predicted by Eq. (9). Repeating the calculation, but now setting $\Delta Q_{\rm jet}$ to its jovian value, the 3 vortices remain trapped in the Rossby wave trough, and they do not merge (Fig. 22). The calculations are sensitive to $\Gamma_{\rm C}$. If it is too large, the three vortices escape from the trough and spread apart; if too small the cyclone hops and the two anticyclones merge. Our calculations show that the vortices remain trapped without merging only for $-4.0 \times 10^2 < \Gamma_{\rm C} < -3.8 \times 10^2$ km^2 s^{-1}. Fig. 22 was computed with $\Gamma_{\rm C} = -3.9 \times 10^2$ km^2 s^{-1} and a cyclone area of 8.2×10^6 km^2.

The 3 vortices sharing the same Rossby wave trough do not maintain fixed distances from each other. The intervening cyclone oscillates back and forth between the two white ovals. When it comes close to a white oval and is repelled, strong tides can be raised on it by the white oval. Fig. 6 from *Galileo* is similar to many frames in our numerical simula-

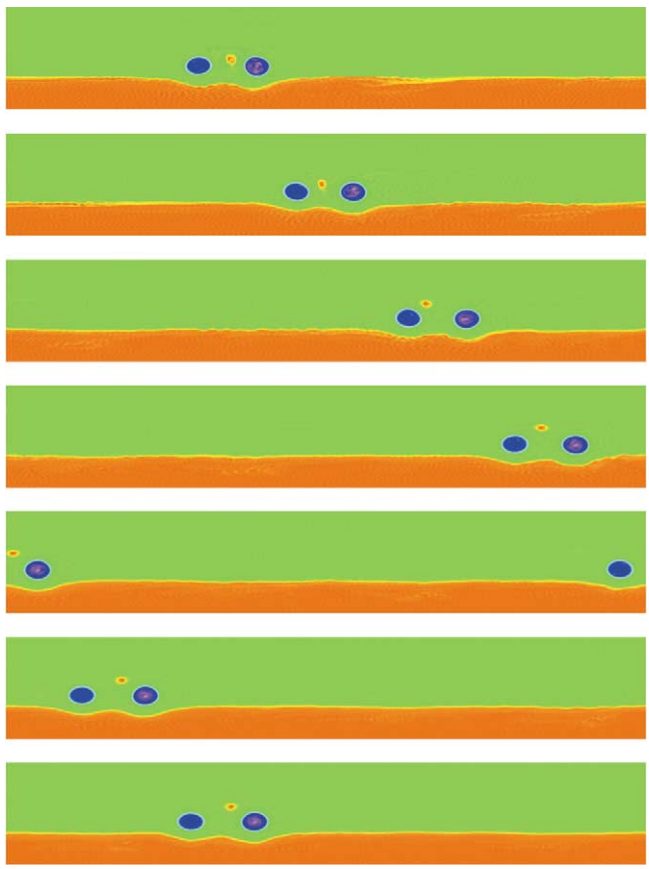

Fig. 22. Same as described in the legend to Fig. 21 but with $\Delta Q_{\rm jet}$ set equal to its jovian value. The eastward jet, which supports the Rossby wave, is shown by a yellow line and is deformed south of the 3 vortices. The vortices neither spread apart nor merge.

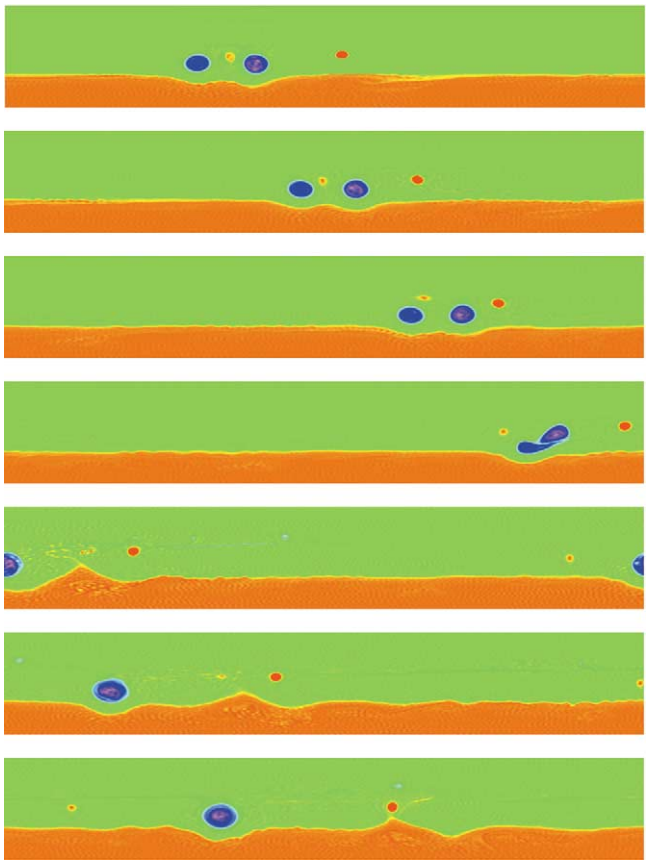

Fig. 23. Same as described in the legend to Fig. 21, but now we initially include a small, (red) cyclone 20,000 km to the east of the Kármán vortex street fragment, well outside the Rossby wave's trough. The 3 vortices in the trough drift eastward at approximately 1 m^{-1} and interact with the small cyclone. The cyclone provides enough repulsion to force the intervening cyclone to hop to the west, allowing the two anticyclones to merge.

tions. White oval BC (which creates a counterclockwise flow around itself) stretches the cyclone C2 and looks as if it will pull a filament south of it. In our calculations we find that the cyclone stretches southward, but does not break into pieces. Neither do we ever see cyclones hop south of an anticyclone. If the flow in Fig. 6 acts similar to our simulations, then C2 will be pushed back toward DE. Before two anticyclones merge, C2 carries out a preferred hop north and west over DE. (The large, white vortex to the south of BC in Fig. 6 is an anticyclone and part of the row of anticyclones at 41°. Although it was reported (Simon et al., 1998) that a vortex pair at 41° was responsible for producing the tail of the cyclone in the figure, we doubt that it could do that.)

5.3. Merger epoch (1997–2000)

We agree with Simon (private communication, 1998) that in September or October of 1997, white oval FA merged with the small anticyclone WO1. (However, we think that this merger was inconsequential to the merger of BC and DE.) We propose that the FA–WO1 merger was preceded by cyclone C4 hopping westward to the north of FA. This hop placed FA adjacent to WO1 and they quickly merged. We believe that C4 survived until at least November 1997 (Fig. 5) where it is visible as a filamentary region between WO2 and FA + WO1 (possibly having merged with any other cyclone that was previously at that location). Unlike Simon (private communication, 1998), we also believe that C3 was also still present.

Fig. 4 shows that prior to the merger of BC and DE the cluster of trapped vortices was drifting eastward at approximately 1 m s^{-1} into cyclone C1. We propose that in late 1997, BC and C1 attained their point of closest approach and that the cyclonic flow of C1 drove BC northward. We argue the interaction occurred prior to November 1997 because Fig. 5 taken in that month shows BC slightly to the north of DE, while it was south of DE on 21 October 1996 (Fig. 4). This interaction with C1 allowed C2, the cyclone between DE and BC, to hop westward to the north of DE where it merged with C3. The merger between BC and DE was most likely completed by February 1998. Although Simon (private communication, 1998) believes that the bright elliptical cyclone between FA + WO1 and BC + DE in Fig. 7 is C2, we believe it is more appropriately labeled as C2 + C3.

The simulation that led to our scenario of how BC and DE merged is shown in Fig. 23. The initial flow has the same 3 vortices and Rossby wave trough as in Fig. 22, but we now also include a small cyclone (to model C1 in Fig. 5) 20,000 km to the east of the Kármán vortex street fragment, well outside the Rossby wave's trough. The 3 vortices drifts eastward and interact with C1, which provides enough repulsion to force the intervening cyclone C2 to carry out a preferred 3-body hop westward to the north of the anticyclone on its westward side. The two adjacent anticyclones then merge in approximately one vortex turn-around time. Starting at the time of closest approach with the eastern cyclone, the merger is finished in 50 days. The merged white oval BC + DE merged with FA in 2000 in a process that took 3 or more weeks (Sánchez-Lavega et al., 2000). This is consistent with our simulations. After white ovals BC and DE merged, the combined vortex had nearly twice the circulation of white oval FA. Our simulations show that a trio of vortices, like FA, C2 + C3, and BC + DE, in which the circulations of the two end anticyclones are asymmetric is not very stable and that a preferred 3-body hop will occur, resulting in the merger of the two anticyclones. It was reported that C2 + C3 disappeared before the merger in 2000 (Sánchez-Lavega et al., 2000). We think it more likely that there was a window in time prior to the merger when the cyclone C2 + C3 was not spatially closely confined between its surrounding anticyclones. During that window, its cloud pattern changed making it difficult to see (Appendix B) in any images that were taken at that time.

6. Conclusions

Using QG theory and equations, we have been able to explain the behavior of the white ovals from the time of their formation in 1939 to their merger in 1998. By assuming that they were the anticyclonic row of a Kármán vortex street, we can understand why from 1940 to 1994 they drifted eastward (and slowly northward) and oscillated longitudinally and why they sometimes came within a diameter of each other before being "repelled," but never merged. By assuming that the Kármán vortex street was trapped in the trough of a Rossby wave between 1994 and 1997, we can explain how the white ovals, along with 2 weaker anticyclones, and the intervening cyclones, drifted as a group with only a diameter or so spacing between them without spreading apart and without merging. By assuming the group drifted into a small cyclone to its east, we can understand the merger of white ovals BC and DE and the merger of white ovals BC + DE and FA. Through numerical simulations we supplied quantitative details of how vortices "hop" over each other and merge with their new neighbors.

We now address the implications of this work for the fate of the remaining white oval and other jovian vortices. We conjecture that cyclone C2 + C3 did not disappear (Sánchez-Lavega et al., 2000) but instead hopped north and west over FA and merged with C4 and that it would be useful to look for an image of C2 + C3 + C4 to the west of the surviving white oval. It is our conjecture that cyclones are not ephemeral; they are just difficult to detect by looking at their associated clouds unless the cyclone and its cloud are compressed between two anticyclones (Appendix A). Thus, we believe it would be useful to search for images of C2 + C3 just prior to the merger of FA and BC + DE when it had not yet hopped to the north and west over FA and might be visible because its clouds were compressed between FA and BC + DE. We feel that the surviving white oval is stable and that it will not fade back into the zonal band from which the 3 white ovals sprang in 1939 (as suggest by Sanchez-Lavega et al., 2000). If the white ovals formed from a Kelvin–Helmholtz instability of the zonal flow—as in the simulations of Dowling and Ingersoll (1989)—this would require making a linear instability go backward in time. A more likely scenario, in our opinion, is that the zonal flow near FA + BC + DE and C2 + C3 + C4 will fill up with 2 or 3 other vortex pairs as it has in the past (Rogers, 1995).

We have argued that vortices moving with small differential velocities do not merge unless they first become trapped in a Rossby wave. This raises the question of how vortices become trapped. According to our numerical simulations, there are three ways in which vortices can become trapped. The strength ΔQ_{jet} of the potential vorticity jump of the eastward jet could increase, but this is unlikely since it is constrained by the homogenization of potential vorticity between eastward jets. Another possibility is that the white ovals could have moved (or other jovian anticyclones will move) southward closer to the eastward jet, but this would be contrary both to the white ovals' observational history and to theoretical predictions (Humphreys, 2000). The most likely way for the White Ovals, or any Kármán vortex street fragment, to have become trapped is if the circulations of the intervening cyclones became weaker. There is a critical value, above which trapping is impossible (Section 5.2). Historically the white ovals have lost area and—we therefore presume—circulation. Humphreys has shown numerically that both cyclones and anticyclones lose circulation due to the ambient turbulence of the atmosphere (Humphreys, 2000). Because the areas of the clouds associated with the white ovals was decreasing, Rogers (1995) predicted that they would eventually disappear. We would now argue that the decrease in area was indicative of loss of circulation in all of the vortices of the Kármán vortex street. The loss in the cyclones did not lead to the disappearance or enhanced dissipation of the white ovals, but instead to their trapping and mergers.

We can apply these ideas to other jovian vortices. The Kármán vortex street at 41°S is a good example. In 1979 it had 12 cyclone/anticyclone pairs; in 1996 it had 6. We argue that the cyclones lost circulation until one or more pairs became trapped in a Rossby wave, then the vortices underwent a "preferred 3-body hop," and then two cyclones and two anticyclones merged. The process repeated until only 6 pairs remained.

The counterexample to our statement that all long-lived jovian vortices are parts of Kármán vortex streets in the Great Red Spot at 22.4°S. We argue that a Kármán vortex street has not formed there because the accompanying row of cyclones would be north of the westward jet that is north of the Red Spot. These latitudes are too close to the equator for the Coriolis force to be large enough to make the flow 2-dimensional or to obey the shallow-water equations. Observations show that near the equator the character of the jovian flow changes, looking much more turbulent and three-dimensional, an environment where vortices do not survive for long. Without an accompanying row of cyclones, we have argued (Section 3.4) that it is impossible to have more than one long-lived anticyclone at the same latitude. Thus, there is only one Great Red Spot and it could not (as has been conjectured by Sanchez-Lavega et al., 2000) have been created from the merger of two or more large, long-lived vortices that were once part of a Kármán vortex street.

We believe that to make progress in understanding the dynamics of the jovian atmosphere, it will be necessary to compute jovian velocity fields from images rather than studying cloud patterns. This is feasible both with satellite images and with ground-based telescopes with adaptive optics (Gibbard et al., 1999). For example, denoting the boundaries of belts and zones as the locations of the eastward and westward jets (which depend on longitude and time) rather than cloud color would go a long way toward clarifying the atmosphere's dynamics. With velocity fields, cyclones can be reliably detected; their associated clouds

are not reliable indicators of vorticity or potential vorticity. With velocity fields, the behavior of cyclones, as well as anticyclones, could be recorded over long periods of time. With these data, it could be determined whether all long-lived vortices (except the Red Spot) are parts of Kármán vortex streets and whether the instances in which the velocity between two anticyclones changes sign always correspond to a close encounter between one of the anticyclones and a cyclone.

Acknowledgments

We thank the Stanford Center for Turbulence Research, NASA Origins Program (NAG5-10664) and NSF Astronomy (AST0098465) and Physics (PHY0078705) Programs and LANL (37336-001-01 2K) for support. Computations were done through an NPACI award at the NSF-funded San Diego Supercomputer Center.

Appendix A

Cyclones and the relation between clouds and dynamics

There is no theoretical argument against long-lived jovian cyclones. (The intermediate geostrophic theory prohibits them, but since intermediate–geostrophic anticyclones rotate rapidly at their centers and look qualitatively nonjovian (Yamagata and Williams, 1984), we do not consider this theory pertinent to the jovian atmosphere.) With the QG equations, cyclones and anticyclones are degenerate and have identical properties. The SW equations break the degeneracy. Cyclones are weaker, but not necessarily any less robust. In any case, we have argued (Marcus, 1993) that the QG limit of the SW equations is valid if Ro $(L/L_r)^2 \ll 1$, where Ro is the Rossby number (approximately $\sim$0.1 for the cyclones associated with the white ovals), $L_r \simeq 1900$ km is the deformation radius, and L is the characteristic length over which the velocity in the cyclones changes (which is often much smaller than the diameter of the vortex when the q within a vortex is nearly uniform). Using Appendix B, $L \simeq 1900$ km for the cyclones. Thus we expect the cyclones to be QG.

It should be noted that jovian cyclones typically are weaker than the anticyclones, but this does not violate QG theory, which treats them as equals. The formation of vortices is ageostrophic (since neither SW or QG theory allows q to be created or destroyed). It has been conjectured that large vortices are created from the repeated mergers of small ones, which in turn are created by atmospheric upwelling and downwelling. The rate of creation of anticyclonic (cyclonic) vorticity is directly proportional to the velocity of the upwelling (downwelling). If upwelling were concentrated to small areas associated with overshooting plumes from convection beneath the weather layer, and if the return downwelling was weaker and spread out over a larger area, then strong anticyclones and weak cyclones would be created.

Although the dynamics of QG cyclones and anticyclones are the same, their associated clouds are not. Simulations of jovian clouds (Graves, 1993) showed that the clouds of the anticyclones were compact and elliptical, while those of the cyclones looked like "filamentary regions"—wispy, tangled, and not circumferential around the cyclones. Because the clouds of the cyclones look different from the closed streamlines expected of a laminar, coherent vortex, whereas the clouds of anticyclones have a more suggestive vortical appearance, it was argued that cyclones cannot be long-lived or coherent (Antipov et al., 1990). However clouds do not coincide with streamlines in a time-dependent flow. Clouds correspond to particle paths (for example, of NH_3 ice crystals that make up the clouds). Turbulent cyclones and anticyclones can have anomalous q and streamlines that are mirror images, yet their associated Lagrangian particle (i.e., ice) paths are not if the regions where particles are created and destroyed are correlated with the flow's vorticity. Graves' simulation of jovian clouds (1993) created Lagrangian particles where the vorticity was anticyclonic (corresponding to upwelling, which in the subadiabatic jovian atmosphere cools the ambient atmosphere (Flasar et al., 1981) and creates ice) and destroyed them where the flow was cyclonic (where the ice melts). The resulting cloud patterns differed from the streamlines: elliptical clouds formed over anticyclones and filamentary, disorganized clouds over cyclones. The clouds associated with the anticyclones coincided with their regions of their anomalous q, but the clouds of the cyclones generally covered a much larger area. Our point is that one must be careful in inferring vortex dynamics from cloud morphologies.

Appendix B

Determination of vortex area and circulation

When velocity fields were available, the areas of the white ovals' anomalous q were determined as follows. The locations of the two extrema of the north–south velocities along the white ovals' semi-major (east–west) axis were found. The area inside the streamline connecting these two locations was used as the area of the white oval. We found that this area was nearly identical to the area of the elliptical cloud covering the white oval. In cases where the velocity field was not available we used the area of the associated cloud as the area of the of the anomalous q. The circulations of the white ovals were determined by adjusting the values until the aspect ratio (minor diameter divided by the major diameter) of our simulated vortex was the same as that of the observed white oval. As reported earlier (Marcus, 1993),

the aspect ratio is a monotonic and sensitive function of the ratio of the circulation to the ambient shear. The q within the white oval was assumed to be uniform over the vortex. For the cyclones, we used the areas and circulations that we determined during the Pre–merger Epoch. We assume that during that time, the area of the anomalous q was the same as the cloud (cf. Fig. 6). The range of circulation that a cyclone can have and remain trapped by a Rossby wave is small. If the circulation is too large, the vortices will not be confined; if it is too small, the anticyclones merge. We chose the middle of the range as the cyclone's circulation. The strength of the potential vorticity jump at the eastward jet south of the white ovals was determined as follows. We assumed that the jovian q is a step function decreasing from the north to south poles and that the q was uniform between the eastward jets. Thus the jump in q at the eastward jet is $\Delta Q_{\text{jet}} = f(y_{\text{n}}) - f(y_{\text{s}})$, where f is the Coriolis parameter and y_{n} (or y_{s}) is the latitude halfway between the eastward jet and its neighboring eastward jet on its northern (southern) side.

References

Antipov, S.V., Nezlin, M.V., Snezhkin, E.N., Trubnikov, A.S., 1990. Great Red Spot models. Nature 343, 516–517.

Beebe, R.F., Orton, G.S., West, R.A. 1989. Time-variable nature of the jovian cloud properties and thermal structure: an observational perspective, in: Belton, M.J.S, West, R.A., Rahe, J. (Eds.), Time-Variable Phenomena in the Jovian System, NASA, SP-494, pp. 245–343.

Cho, J.Y.-K., Polvani, L.M., 1996. The emergence of jets and vortices in freely evolving, shallow-water turbulence on a sphere. Phys. Fluids 8, 1531–1552.

Dowling, T.E., Ingersoll, A.P., 1988. Potential vorticity and layer thickness variations in the flow around Jupiter's Great Red Spot and White Oval BC. J. Atmos. Sci. 45, 1380–1396.

Dowling, T.E., Ingersoll, A.P., 1989. Jupiter's Great Red Spot as a shallow water system. J. Atmos. Sci. 46, 3256–3278.

Flasar, F.M., Conrath, B.J., Pirraglia, J.A., Clark, P.C., French, R.G., Gierasch, P.J., 1981. Thermal structure and dynamics of the jovian atmosphere: 1. The Great Red Spot. J. Geophys. Res. 86, 8759–8767.

Gibbard, S.G., Macintosh, B., Gavel, D., Max, C.E., de Pater, I., Ghez, A.M., Young, E.F., McKay, C.P., 1999. Titan: high-resolution speckle images from the Keck telescope. Icarus 139, 189–201.

Graves, C., 1993. Simulation of Jovian Clouds. Master's thesis. University of California, Berkeley.

Humphreys, T.D., 2000. Jovian Kármán Vortex Streets as Attractors in Turbulent Zonal Flow. Ph.D. thesis. University of California, Berkeley.

Ingersoll, A.P. 1996. Structure and dynamics of Jupiter's atmosphere after Galileo, in: Proceedings of the American Geophysical Union, San Francisco.

Ingersoll, A.P., Cuong, P.G., 1981. Numerical model of long-lived jovian vortices. J. Atmos. Sci. 38, 2067–2076.

Kim, S., 1996. Dynamics of Great Red Spot and Jovian Zonal Flows, Ph.D. thesis. University of California, Berkeley.

Kuehn, D.M., Beebe, R.F., 1989. A deceleration of the White Ovals. Bull. Am. Astron. Soc. 21, 945.

Limaye, S.S., 1986. Jupiter: new estimates of the mean zonal flow at the cloud level. Icarus 65, 335–352.

MacLow, M.-M., Ingersoll, A.P., 1986. Merging of vortices in the atmosphere of Jupiter: an analysis of Voyager images. Icarus 65, 353–369.

Marcus, P.S., 1988. Numerical simulation of Jupiter's Great Red Spot. Nature 331, 693–696.

Marcus, P.S., 1990. Vortex dynamics in a shearing zonal flow. J. Fluid Mech. 215, 393–430.

Marcus, P.S., 1993. Jupiter's Great Red Spot and other vortices. Annu. Rev. Astron. Astrophy. 31, 523–573.

Marcus, P.S., Lee, C., 1994. The Great Red Spot and zonal winds as a self-consistent, one-layer, geostrophic flow. Chaos 4, 269–286.

Marcus, P.S., Kundu, T., Lee, C., 2000. Vortex dynamics and zonal flows. Phys. Plasmas 7, 1630–1640.

McDowell, S., Rhines, P., Keffer, T., 1982. North Atlantic potential vorticity and its relation to the general circulation. J. Phys. Oceanogr. 12, 1417–1436.

Mitchell, J.L., Beebe, R.F., Ingersoll, A.P., Garneau, G.W., 1981. Flow fields within Jupiter's Great Red Spot and White Oval BC. J. Geophys. Res. 86, 8751–8757.

Nezlin, M., 1994. Rossby solitary vortices, on giant planets and in the laboratory. Chaos 4, 187–202.

Pedlosky, J., 1987. Geophysical Fluid Dynamics. Springer-Verlag, New York.

Rogers, J.H., 1995. The Giant Planet Jupiter. Cambridge Univ. Press, Cambridge.

Rogers, J., Herbert, D., 1991. The three White Ovals and adjacent belts in the South Temperate region of Jupiter, 1940–1990. J. Br. Astron. Assoc. 101, 351–360.

Sánchez-Lavega, A., Rojas, J.F., Hueso, R., Lecacheux, J., Colas, F., Acarreta, J.R., Miyazaki, I., Parker, D., 1999. Interaction of Jovian White Ovals BC and DE in 1998 from Earth-Based Observations in the Visual Range. Icarus 142, 116–124.

Sánchez-Lavega, A., and 12 colleagues, 2000. The merger of two giant anticyclones in the atmosphere of jupiter. Bull. Am. Astron. Assoc. 32, 401 (abstract).

Sato, T., 1974. Statistical establishment of the repulsive force between the long-enduring White Ovals in the South Temperate Zone on Jupiter. J. Brit. Astron. Assoc. 84, 439–442.

Simon, A.A., Beebe, R.F., Gierasch, P.J., Vasavada, A.R., Belton, M.J.S., 1998. Global context of the Galileo-E6 observations of Jupiter's white ovals. Icarus 135, 220–229 and the Galileo Imaging Team.

Smith, B.A., and 12 colleagues, 1979. The Jupiter system through the eyes of Voyager 1. Science 204, 951–972.

Solomon, T.H., Holloway, W.J., Swinney, H.L., 1993. Shear flow instabilities and rossby waves in barotroipic flow in a rotating annulus. Phys. Fluids 5, 1971–1982.

Sommeria, J., Meyers, S.D., Swinney, H.L., 1989. Laboratory model of a planetary eastward jet. Nature 337, 58–61.

Sutyrin, G., 1994. Long lived planetary vortices and their evolution: conservative intermediate geostropohic model. Chaos 4, 203–212.

Vasavada, A.V., Ingersoll, A.P., Banfield, D., Bell, M., Gierasch, P.J., Belton, M.J.S., Klassen, K.P., Jong, E.D., Breneman, H.H., Jones, T.J., Kaufman, J.M., Magee, K.P., Senske, D.A., 1998. Galileo imaging of Jupiter's atmosphere: the Great Red Spot, equitorial region, and White Ovals. Icarus 135, 265–275.

Yamagata, T., Williams, G.P., 1984. Geostrophic regimes, intermediate solitary vortices and jovian eddies. J. Atmos. Sci. 41, 453–478.